I. INTRODUCTION

A. PROBLEM OVERVIEW

The increasing demands of using submersible vehicles for more complex and demanding missions, force us to use a variety of methods, mathematical models, and assumptions for the study of their dynamic interactions and responses. This study is important in order to enhance vehicle operations. Typically, linearization of the equations of motion around nominal straight line level flight paths along with eigenvalue analysis can be employed (Arentzen and Mandel, 1960), (Clayton and Bishop, 1982), (Feldman,1987). A simple but efficient stability criterion $Gv > 0$ can be obtained where the stability index G_v is function of the hydrodynamic coefficients in heave and pitch. Values for the stability index can be computed by,

$$G_v = 1 - \frac{M_w(Z_q + m)}{Z_w M_q} \; . \tag{1}$$

This index is analogous to the familiar stability coefficient for horizontal plane maneuvering and can be thought of as a high speed approximation where the effect of the metacentric restoring moment is minimal (Papadimitriou,1994). If the value of G_v is greater than zero, the vehicle is dynamically stable. As it has been established in previous studies (Papoulias and Papadimitriou, 1995) though, this is only a sufficient, and rather conservative condition for stability. Nevertheless, it is widely used and its value is indicative of vertical plane stability for any new design. We should keep in mind, however, that the condition

$G_v < 0$ indicates a divergent loss of stability which is quite uncommon in the vertical plane. Most modern submarines exhibit a flutter–like instability at high speed, which can not be analyzed using the above simplified index. Divergent motions may develop in combined six degrees of freedom (Papoulias *et al*, 1993) and their occurrence can not be analyzed by a single stability index. Previous work (Papadimitriou, 1994) was limited to a single body with fixed hydrodynamic coefficients. In this work, we expand by allowing the geometry of the body and thus its hydrodynamic properties to vary.

B. THESIS OUTLINE

Previous work (Papoulias and Papadimitriou, 1995) analyzed the problem of stability of motion with controls fixed in the vertical plane, with particular emphasis on the mechanism of loss of stability of straight line motion. The closed loop control problem was analyzed in (Papoulias *et al*, 1995). The surge equation was decoupled from heave/pitch through a perturbation series approach (Bender and Orszag, 1978). As was established in (Papadimitriou, 1994) loss of stability occurs in the form of generic bifurcations to periodic solutions (Guckenheimer and Holmes, 1983). Taylor expansions and center manifold approximations were employed in order to isolate the main nonlinear terms that influence system response after the initial loss of stability (Hassard and Wan, 1978). Integral averaging was performed in order to combine the nonlinear terms into a design stability coefficient (Chow and Mallet–Paret, 1977). Some difficulties associated with the nonsmoothness of the absolute value nonlinearities was dealt with by employing the concept of generalized gradient (Clarke, 1983). This was employed as an alternative to the linear/cubic approximation typically used in ship roll motion studies (Dalzell, 1978). The same methodology is applied in this work in order to analyze the sensitivity of the results with respect to geometric characteristics of the body.

Vehicle modeling in this work follows standard notation (Gertler and Hagen, 1976), (Smith *et al*, 1978), and numerical results are presented for a family of bodies of revolution similar to the DARPA SUBOFF model (Roddy, 1990) for which a set of hydrodynamic coefficients and geometric properties is available. This parametric study is conducted utilizing existing semi–empirical methods for the calculation of hydrodynamic coefficients. The methods are based on (Fidler and Smith, 1978), (Humphreys and Watkinson, 1978), (Peterson, 1980) and have been verified in (Wolkerstorfer, 1995). The effects of varying the nose, base, and tail fractions of the body as well its nondimensional volume to length ratio on the hydrodynamic derivatives were studied in (Holmes, 1995) where prediction equations were derived based on curve fitting of the results. These hydrodynamic prediction equations are normalized by taking the SUBOFF model as a baseline. This model has been experimentally validated for angles of attack on the hull between ± 15 deg., while the constant coefficient approximation introduces very little error in time domain simulations (Tinker, 1978). Unless otherwise mentioned, all results in this work are presented in standard dimensionless form with respect to the vehicle length

$L = 4.26$ m, and nominal forward speed $U = 2.44$ m/sec (Papadimitriou, 1994).

II. PROBLEM FORMULATION

A. EQUATIONS OF MOTION

In order to obtain the mathematical model the following assumptions, restrictions, and definitions have to be made:

1. The submersible vehicle motion is restricted in the vertical plane, thus the model consists of coupled nonlinear heave and pitch equations.
2. The coordinate frame is fixed at the vehicle's geometrical center.
3. Vehicle is port/starboard symmetric and neutrally buoyant.
4. Use Newton's equations of motion in dimensionless form.

The nonlinear heave and pitch equations become:

$$
\begin{aligned}
& m(\dot{w} - uq - z_G q^2 - x_G \dot{q}) = Z_{\dot{q}}\dot{q} + Z_{\dot{w}}\dot{w} + Z_q q + Z_w w \\
& \quad -C_D \int_{\text{tail}}^{\text{nose}} b(x)(w - xq)|w - xq|\, dx, \qquad (2) \\
& I_y \dot{q} + m z_G(\dot{u} + wq) - m x_G(\dot{w} - uq) = M_{\dot{q}}\dot{q} + M_{\dot{w}}\dot{w} + M_q q + M_w w \\
& \quad +C_D \int_{\text{tail}}^{\text{nose}} b(x)(w - xq)|w - xq| x\, dx \\
& \quad -x_{GB} W \cos\theta - z_{GB} W \sin\theta, \qquad (3)
\end{aligned}
$$

where $x_{GB} = x_G - x_B$, $z_{GB} = z_G - z_B$, and the rest of the symbols are based on standard notation as shown in Table 1. Without loss of generality we can assume that $z_B = x_B = 0$, so that $x_{GB} = x_G$ and $z_{GB} = z_G$. The cross flow integral terms in these equations become very important for high angles of attack maneuvering, where they provide the primary motion damping. The drag coefficient, C_D, is assumed to be constant throughout the vehicle length for simplicity. This does not affect the qualitative properties of the results that follow. The vehicle pitch rate is,

$$\dot{\theta} = q \; . \tag{4}$$

Dynamic coupling between surge and heave/pitch is present due to coordinate coupling as a result of the nonzero metacentric height. However, it has been shown (Papoulias and Papadimitriou, 1995) that this coupling is of higher order and does not change the linear and nonlinear results that follow.

B. HYDRODYNAMIC COEFFICIENTS

Systematic studies based on semi–empirical methods have resulted in the evaluation of hydrodynamic coefficients for a generic body of revolution in terms of basic geometric properties. Curve fitting revealed that adequate accuracy for initial design can be obtained by equations of the form

$$\begin{aligned} H_C &= A_1 F_n^2 + A_2 F_n F_m + A_3 F_m^2 + A_4 F_n \\ &\quad + A_5 F_m + A_6 + A_7 \left(\frac{V}{L^3} - C \right) \; , \end{aligned}$$

where H_C denotes a given coefficient in its standard nondimensional form, V the underwater volume of the body, L its nominal length, F_n the nose fraction, and F_m the mid–body fraction. The regression coefficients A_i are presented

A_i	regression coefficient
$b(x)$	local beam of the hull
C	nominal value of volumetric coefficient
C_D	quadratic drag coefficient
F_n	nose length fraction
F_m	middle-body length fraction
H_c	given hydrodynamic coefficient
I_y	vehicle mass moment of inertia
K	nonlinear stability coefficient
L	vehicle length
m	vehicle mass
M	pitch moment
M_a	derivative of M with respect to a
q	pitch rate
$\mathbf{T}$	transformation matrix of $\mathbf{x}$ to $\mathbf{z}$
u	forward speed
u_c	critical value of u
V	total volume
w	heave velocity
$\mathbf{x}$	state variables vector, $\mathbf{x} = [\theta, w, q]$
(x_B, z_B)	body fixed coordinates of vehicle center of buoyancy
(x_G, z_G)	body fixed coordinates of vehicle center of gravity
x_{GB}	center of gravity/center of buoyancy separation, $x_G - x_B$
z_{GB}	vehicle metacentric height, $z_G - z_B$
Z	heave force
Z_a	derivative of Z with respect to a
α_{ij}	expansion coefficients of z_3 in terms of z_1, z_2
δ	stern plane deflection
ϵ	criticality difference, $\epsilon = u - u_c$
θ	pitch angle

Table 1: Nomenclature

H_C	A_1	A_2	A_3	A_4	A_5	A_6	A_7
Z_w	-0.0641	-0.1149	-0.0632	$+0.0670$	$+0.0732$	-0.0263	-0.5769
M_w	$+0.0277$	$+0.0499$	$+0.0266$	-0.0283	-0.0301	-0.0056	-1.6357
Z_q	-0.0314	-0.0559	-0.0292	$+0.0310$	$+0.0316$	-0.0091	-0.0880
M_q	-0.0003	$+0.0040$	$+0.0027$	-0.0012	-0.0045	$+0.0006$	-0.1590
$Z_{\dot{w}}$	$+0.0002$	$+0.0007$	$+0.0007$	-0.0008	-0.0016	-0.0144	-1.8067
$M_{\dot{w}}$	-0.0002	-0.0007	-0.0007	$+0.0008$	$+0.0016$	$+0.0144$	$+1.8067$
$M_{\dot{q}}$	-0.0031	-0.0046	-0.0021	$+0.0031$	$+0.0024$	-0.0013	-0.0808

Table 2: Regression coefficients A_i

in Table 2. $Z_{\dot{q}}$ was assumed constant since the semi–empirical techniques failed to compute a reliable value. Basic geometric definitions for the body are presented in Figure 1. The constant C is approximately 8×10^{-3} and is the nominal value for the volumetric coefficient. These expressions are for a body of revolution without appendages and assume parabolic nose, parallel mid–body, and conical tail (Holmes, 1995). Typical ranges of applicability for these regression formulas are 0.05 to 0.25 for F_n, 0.40 to 0.60 for F_m, and 6.0 to 10.0 for V/L^3. Sample results for the above hydrodynamic coefficients versus the nose and mid–body fraction ratios are presented in Figures 2 through 8.

C. DEGREE OF STABILITY

The degree of stability is defined as the largest real part of all eigenvalues of the linearized system of equations (2), (3), and (4). Positive values indicate an unstable system while negative values show stability of forward motion. The degree of stability versus x_{GB} for constant forward speed $u = 0.5$ and different values of z_{GB} is shown in Figures 9 through 12. Based on these results we can

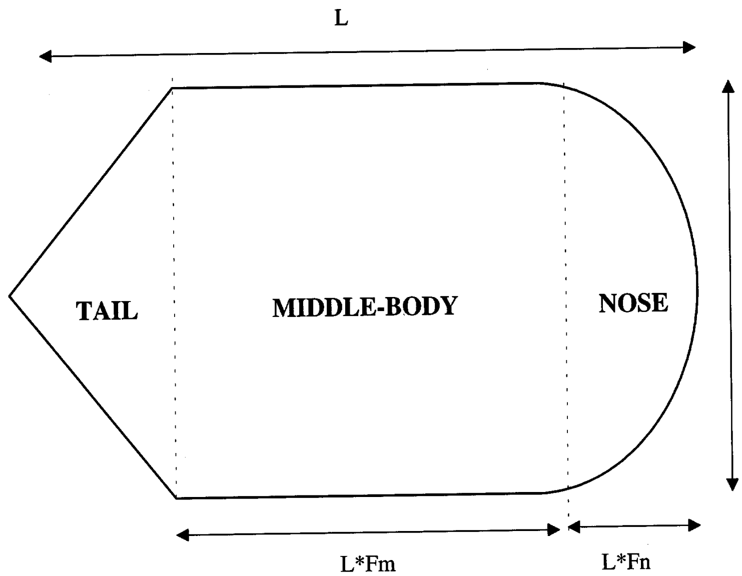

Figure 1: Geometric definitions

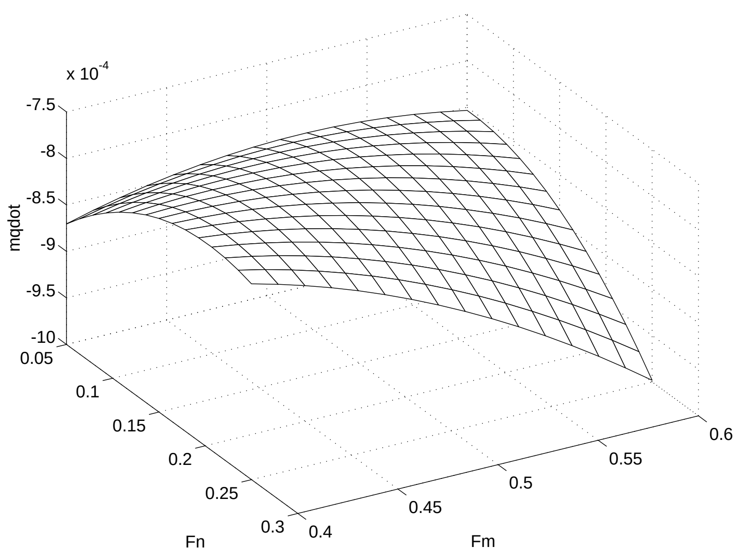

Figure 2: Hydrodynamic coefficient $M_{\dot{q}}$ versus F_n and F_m

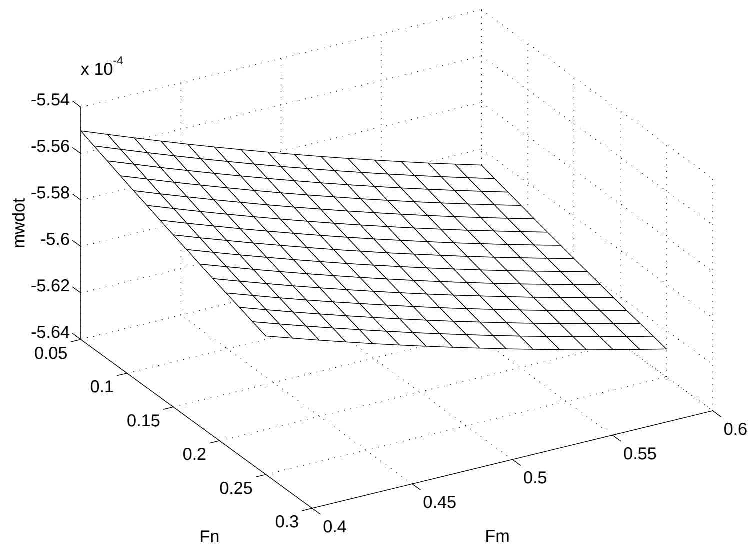

Figure 3: Hydrodynamic coefficient $M_{\dot{w}}$ versus F_n and F_m

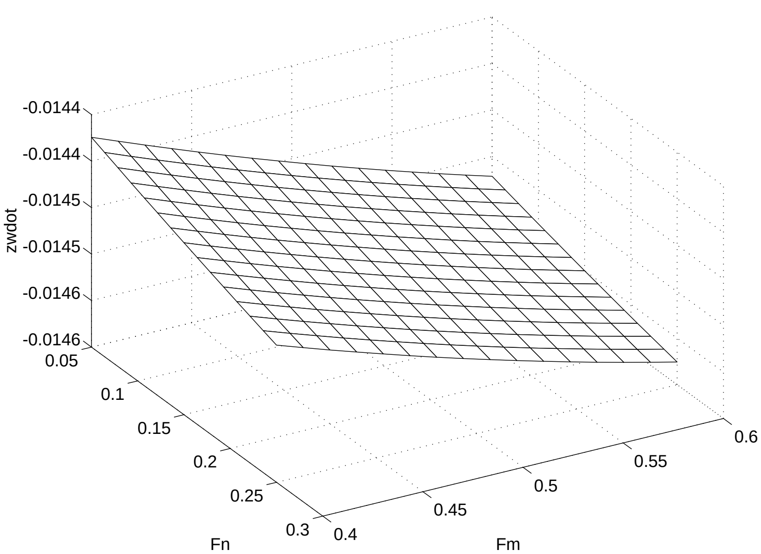

Figure 4: Hydrodynamic coefficient $Z_{\dot{w}}$ versus F_n and F_m

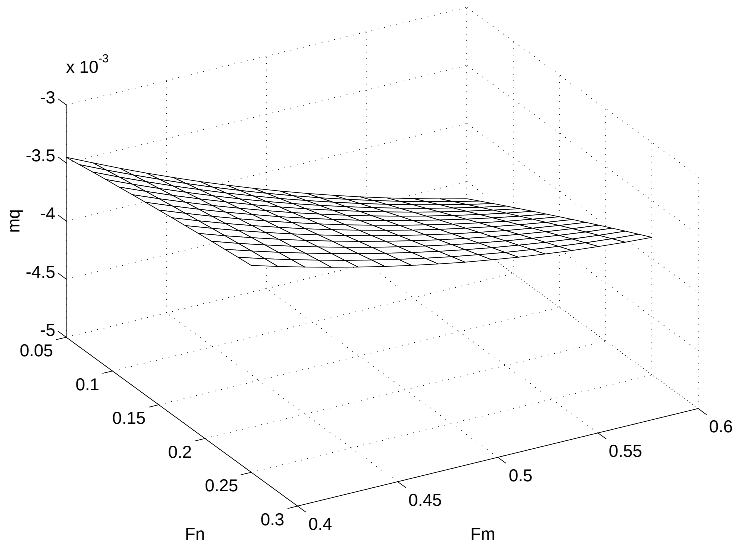

Figure 5: Hydrodynamic coefficient M_q versus F_n and F_m

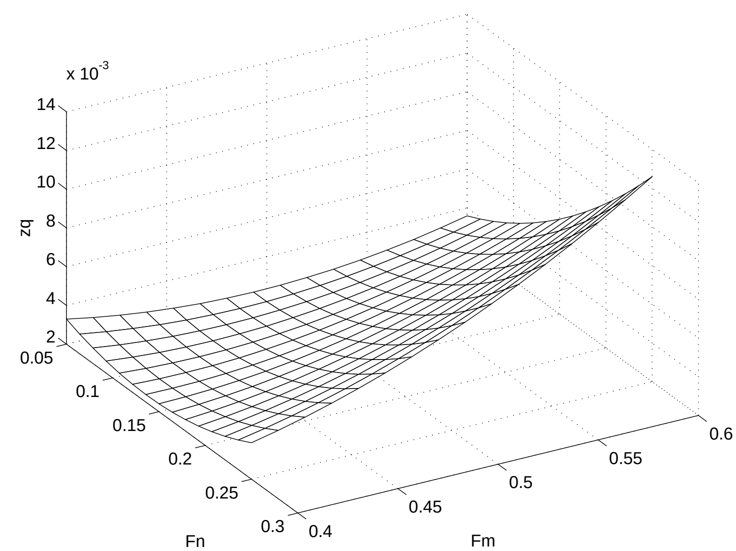

Figure 6: Hydrodynamic coefficient Z_q versus F_n and F_m

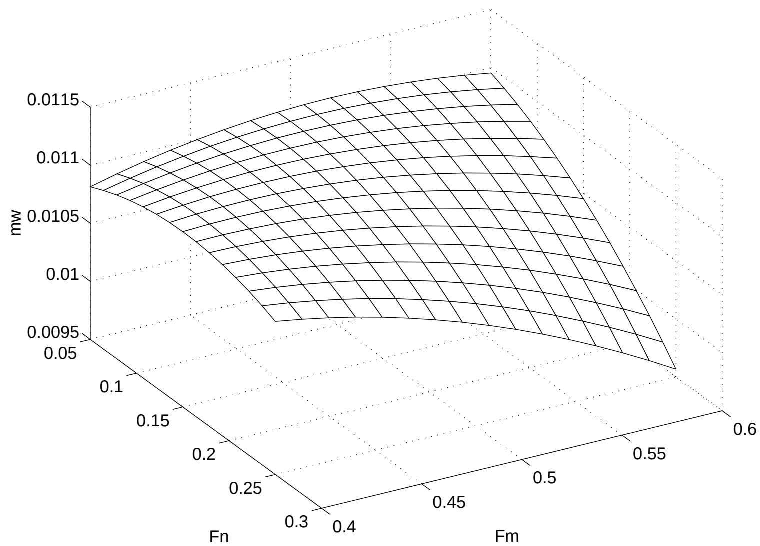

Figure 7: Hydrodynamic coefficient M_w versus F_n and F_m

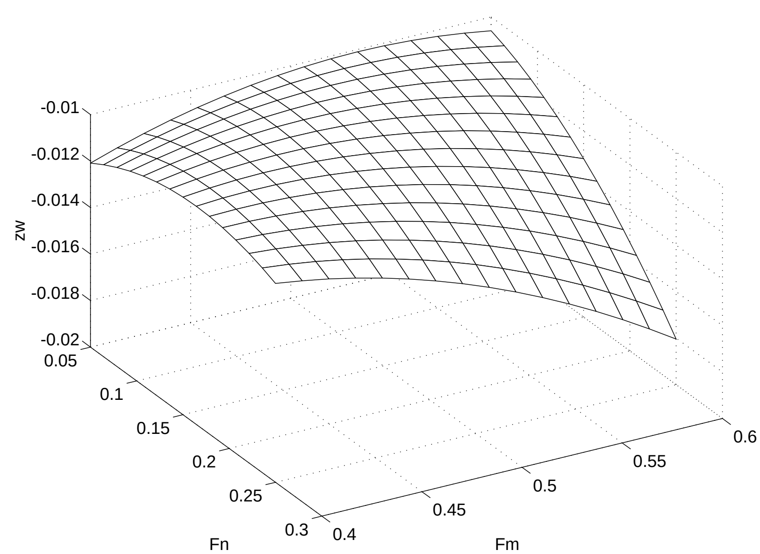

Figure 8: Hydrodynamic coefficient Z_w versus F_n and F_m

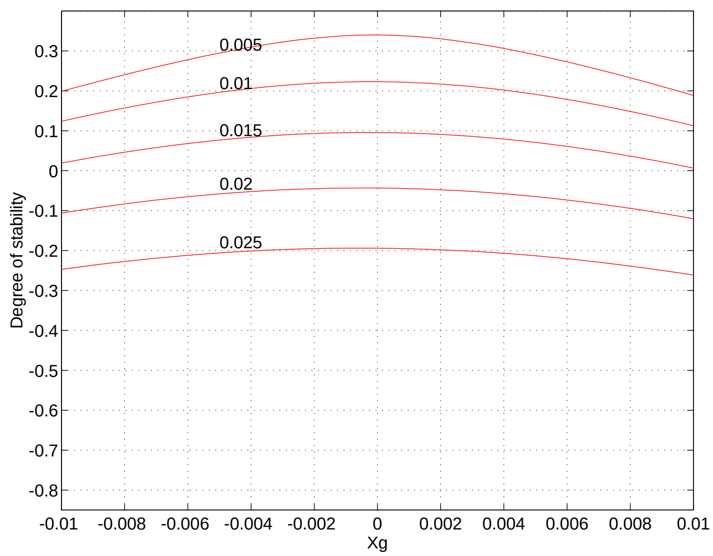

Figure 9: Degree of stability for $u = 0.5$, varying z_{GB}, $F_n = 0.3$, and $F_m = 0.6$

draw the following conclusions:

1. In all cases the vehicle is dynamically more stable as the metacentric height z_{GB} is increased.

2. In all cases the vehicle is dynamically less stable as the separation between the centers of gravity and buoyancy is reduced in absolute value.

3. For constant F_n, increasing values of F_m result in less stable vehicles. This means that a longer tail is beneficial for stability of motion, as expected.

4. The same conclusion holds for constant mid–body ratio F_m and varying nose ratios F_n.

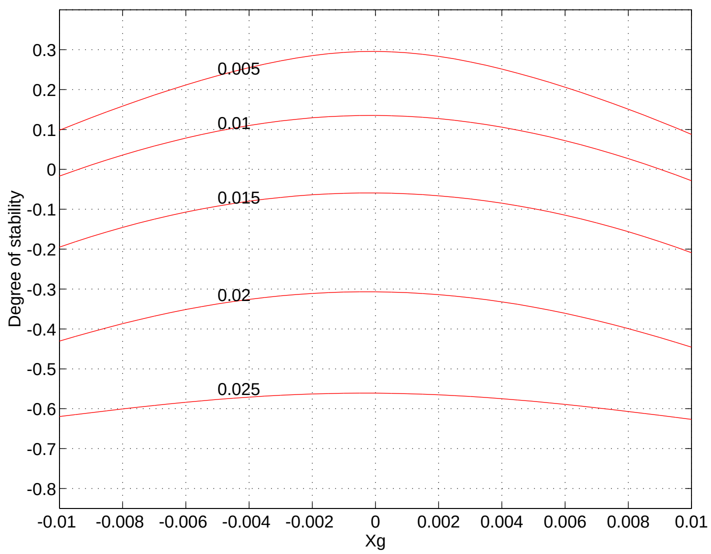

Figure 10: Degree of stability for $u = 0.5$, varying z_{GB}, $F_n = 0.1$, and $F_m = 0.4$

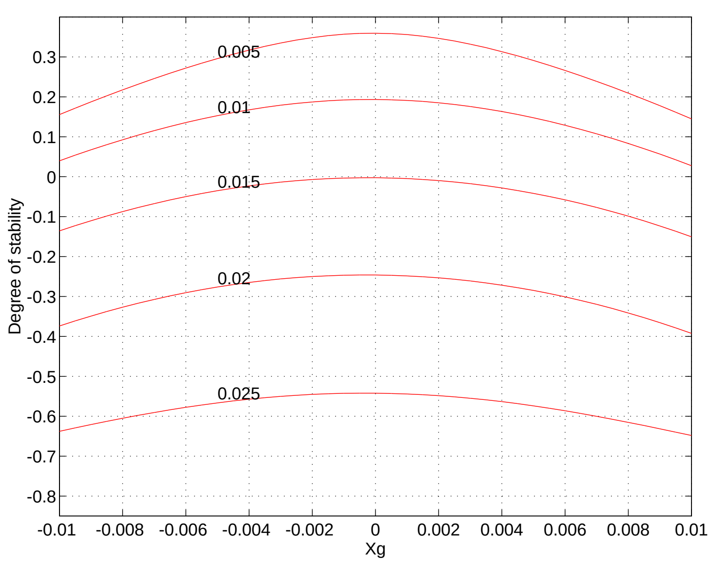

Figure 11: Degree of stability for $u = 0.5$, varying z_{GB}, $F_n = 0.3$, and $F_m = 0.4$

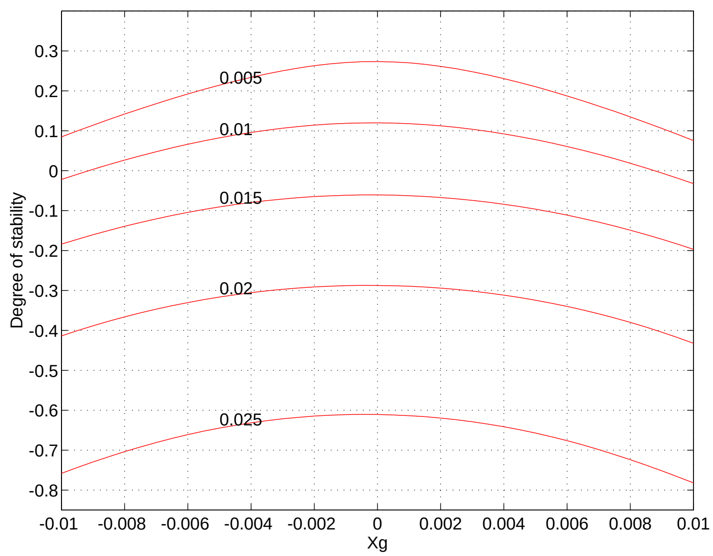

Figure 12: Degree of stability for $u = 0.5$, varying z_{GB}, $F_n = 0.1$, and $F_m = 0.6$

Corresponding results for constant $z_{GB} = 0.015$ and varying forward speeds u are shown in Figures 13 through 16. Similar conclusions as those discussed previously hold in these cases with the following exceptions:

1. For very low forward speeds, the case $x_G = 0$ may be best for stability.

2. For very low speeds, smaller tails may result in more stable configurations.

Combined results for variations in both x_{GB} and u are shown by the mesh plots of Figures 17 through 20. The value of z_{GB} was held constant at 0.015 for all plots. These figures confirm our previous conclusions by presenting the results in more detail.

Figure 21 shows the degree of stability versus F_n and F_m. Both values

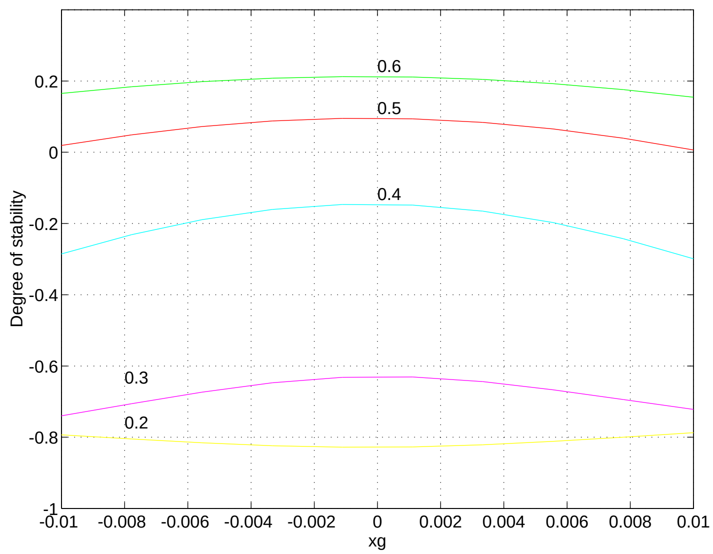

Figure 13: Degree of stability for $z_{GB} = 0.015$, varying u, $F_n = 0.3$, and $F_m = 0.6$

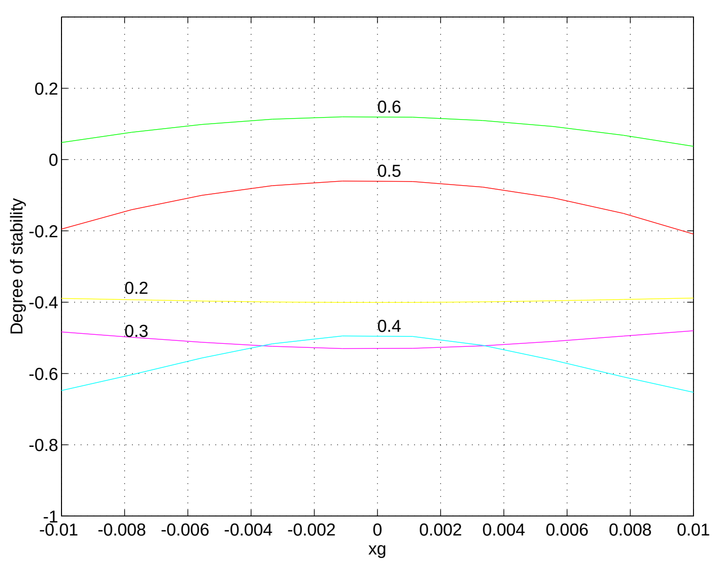

Figure 14: Degree of stability for $z_{GB} = 0.015$, varying u, $F_n = 0.1$, and $F_m = 0.4$

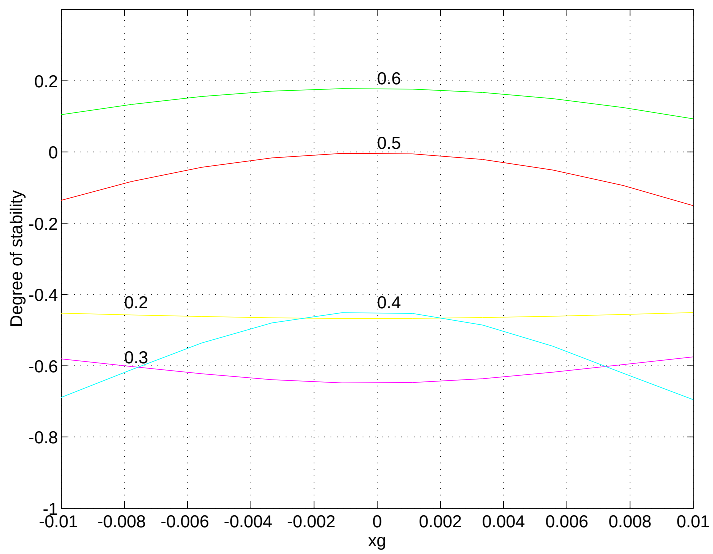

Figure 15: Degree of stability for $z_{GB} = 0.015$, varying u, $F_n = 0.3$, and $F_m = 0.4$

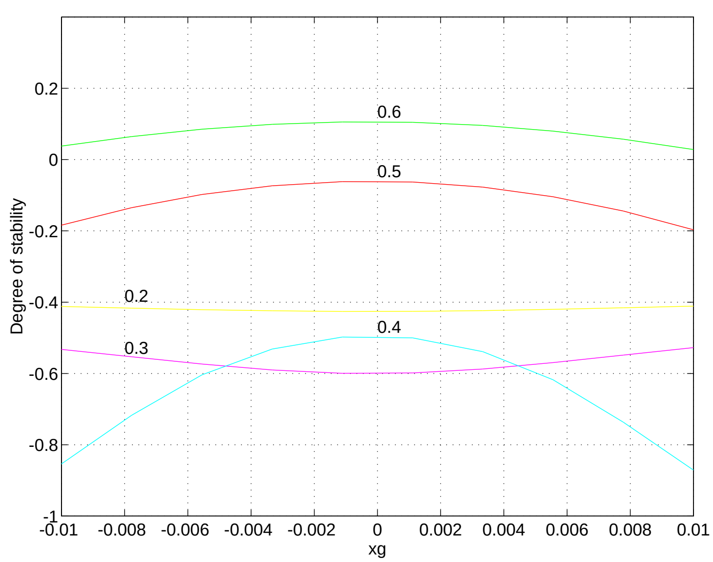

Figure 16: Degree of stability for $z_{GB} = 0.015$, varying u, $F_n = 0.1$, and $F_m = 0.6$

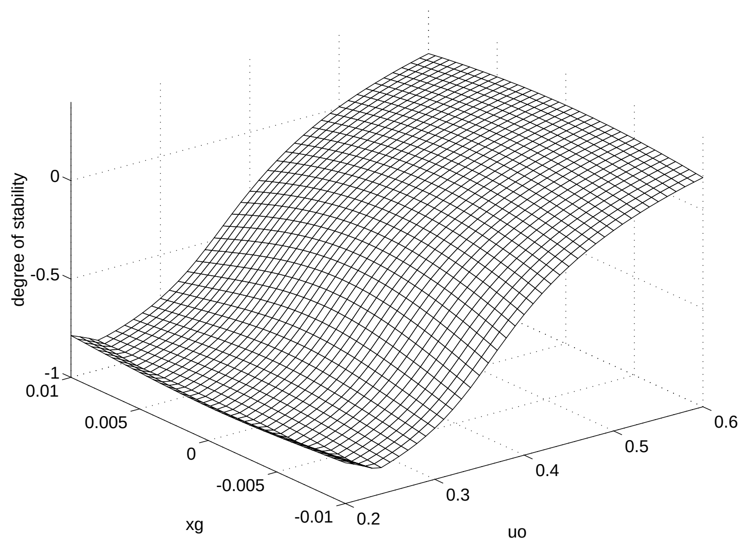

Figure 17: Degree of stability for $F_n = 0.3$ and $F_m = 0.6$

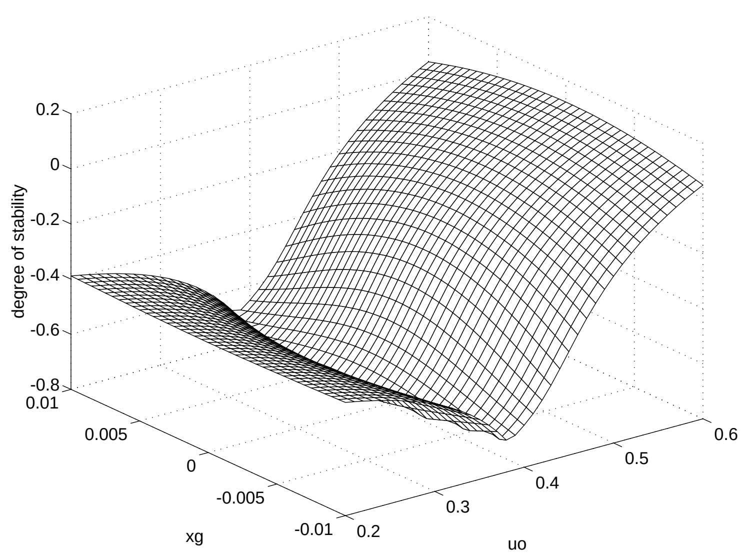

Figure 18: Degree of stability for $F_n = 0.1$ and $F_m = 0.4$

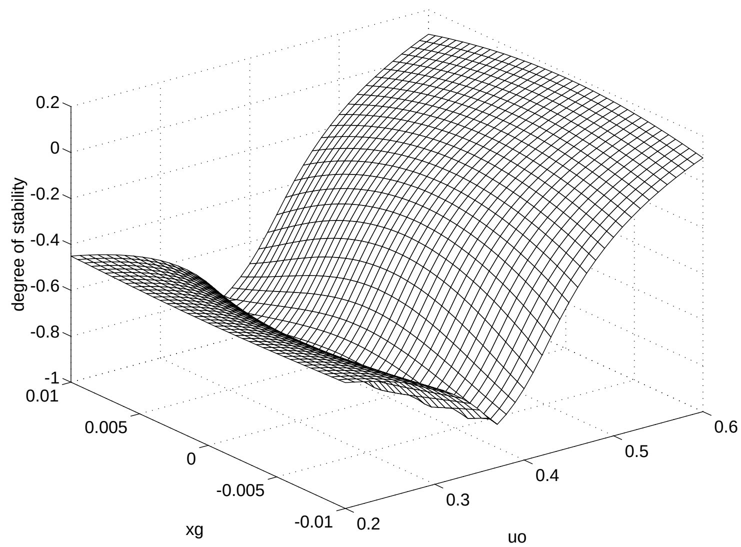

Figure 19: Degree of stability for $F_n = 0.3$ and $F_m = 0.4$

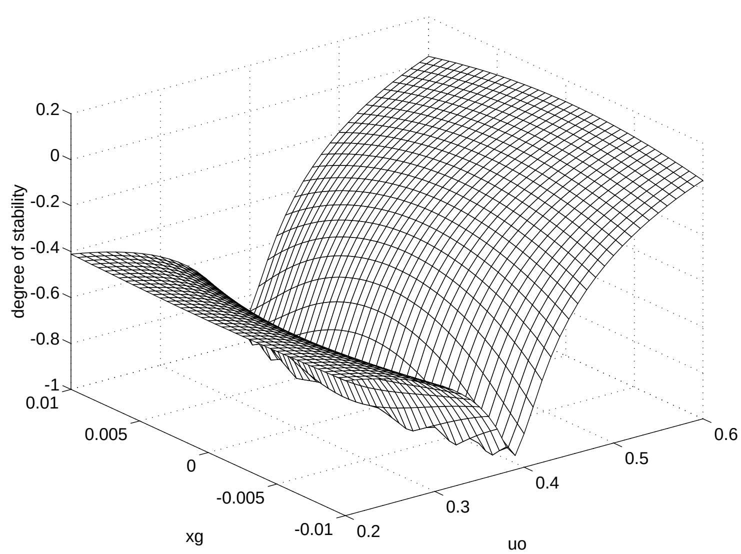

Figure 20: Degree of stability for $F_n = 0.1$ and $F_m = 0.6$

of x_G and z_G were kept constant and equal to 0 and 0.015 respectively. The three surfaces shown correspond to values $u = 0.4, 0.5, 0.6$. The upper one corresponds to $u = 0.6$ while the lower one to $u = 0.4$. It can be seen that the degree of stability becomes more negative for decreasing u, and, generally speaking, for decreasing F_n and F_m.

Figure 22 shows the degree of stability versus F_n and F_m. Both values of forward speed u and z_G were kept constant and equal to 0.5 and 0.015 respectively. The three surfaces shown correspond to values $x_G = -0.01, 0, +0.01$. The upper one corresponds to $x_G = 0.0$ while the lower one to $x_G = +0.01$. It can be seen that the degree of stability becomes more negative for increasing x_G in absolute value, and, generally speaking, for decreasing F_n and F_m.

Figure 23 shows the degree of stability versus F_n and F_m. Both values of forward speed u and x_G were kept constant and equal to 0.5 and 0.0 respectively. The three surfaces shown correspond to values $z_G = +0.005, +0.015, +0.025$. The upper one corresponds to $z_G = +0.005$ while the lower one to $z_G = +0.0025$. It can be seen that the degree of stability becomes more negative for increasing z_G, and, generally speaking, for decreasing F_n and F_m.

D. CRITICAL SPEED

The parameter value where the real part of the dominant complex conjugate pair of eigenvalues crosses zero defines the point where linear stability is lost. This critical point can be computed by considering the characteristic equation

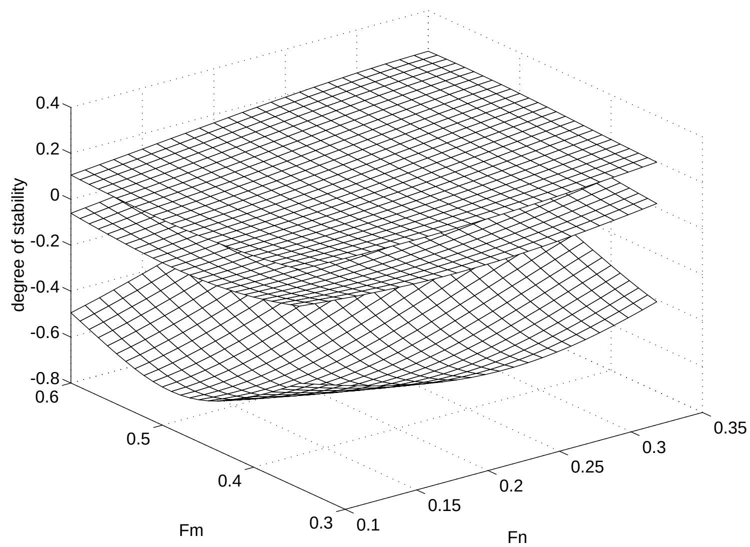

Figure 21: Degree of stability versus F_n and F_m for $x_G = 0$, $z_G = 0.015$, and $u = 0.4, 0.5, 0.6$

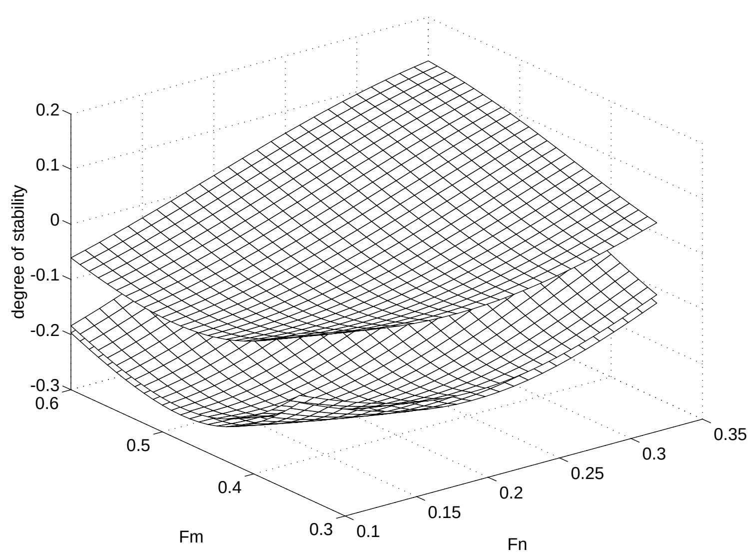

Figure 22: Degree of stability versus F_n and F_m for $u = 0.5$, $z_G = 0.015$, and $x_G = -0.01, 0, +0.01$

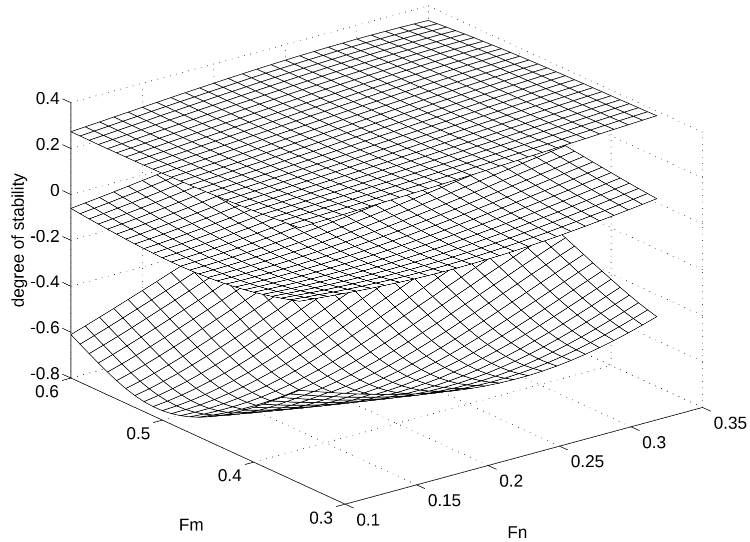

Figure 23: Degree of stability versus F_n and F_m for $u = 0.5$, $x_G = 0$, and $z_G = 0.005, 0.015, 0.025$

of the system (Papadimitriou, 1994). Routh's criterion applied to this can be solved for the dimensionless weight,

$$W = \frac{B_2 C_{2,0}}{A_2 D_{2,1} - B_2 C_{2,1}} \ , \tag{5}$$

where,

$$\begin{aligned} C_{2,0} &= Z_w(M_q - m x_G) - M_w(Z_q + m) \ , \\ C_{2,1} &= (m - Z_{\dot{w}})(z_{GB} \cos\theta_0 - x_{GB} \sin\theta_0) \ , \\ D_{2,1} &= Z_w(x_{GB} \sin\theta_0 - z_{GB} \cos\theta_0) \ . \end{aligned}$$

It should be mentioned that the effect of the forward speed u is embedded into the definition for the dimensionless vehicle weight W through,

$$W \longrightarrow \frac{W}{\frac{1}{2}\rho u^2 L^2} \ . \tag{6}$$

The value of the critical speed u_c can then be evaluated from (5) and (6). Typical results are presented in Figures 24 through 27. A family of critical speeds, u_c, is shown versus x_G with z_G as the parameter of the curves. These results were obtained for a nose fraction $F_n = 0.1, 0.3$ and mid–body fraction $F_m = 0.4, 0.6$. The volumetric coefficient was kept at nominal for all results. Vertical plane motions are stable for forward speeds less than the critical speed. It can be seen that stability is increasing with increasing z_G while $x_G = 0$ is the most conservative condition for stability. Therefore, a vehicle which is stable when properly trimmed will remain stable for off–trim conditions. The fact that a vehicle with a longer aft–body ought to be dynamically more stable is confirmed by comparing the results of Figures 24 and 26 to the results shown in Figures 25 and 27 respectively. It can be seen that the corresponding critical speeds become smaller, thereby reducing the dynamic stability margin, as the nose and mid–body fractions are raised. This trend is consistent for all values of x_G and z_G examined.

Combined plots of the critical speed versus both x_G and z_G are shown in Figures 28 and 29. Figure 28 presents the surfaces for $F_n = 0.3$ and $F_m = 0.4, 0.5, 0.6$. The uppper surface corresponds to $F_m = 0.4$. Figure 29 presents the surfaces for $F_m = 0.5$ and $F_n = 0.1, 0.2, 0.3$. The upper surface corresponds to $F_n = 0.1$.

Combined plots of the critical speed versus both F_n and F_m are shown in Figures 30 through 32. Figure 30 presents the surface when $z_G = 0.0125$ and $x_G = 0$. Figure 31 gives us a comparative view keeping $z_G = 0.0125$ and

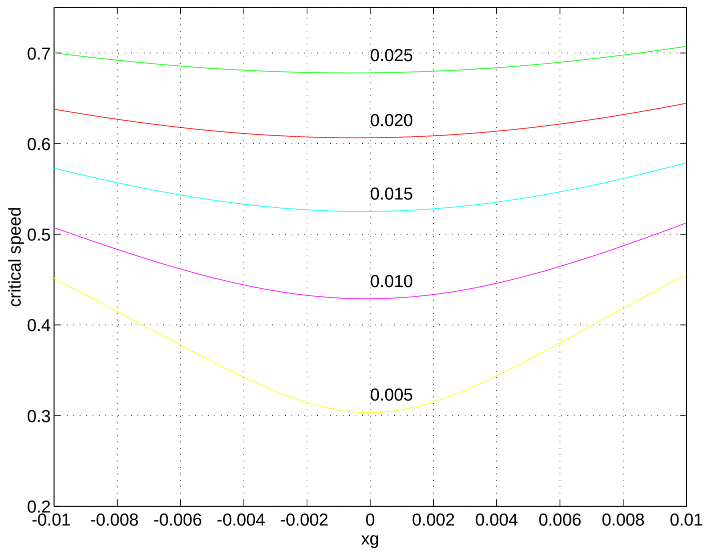

Figure 24: Critical speed versus x_G for $F_n = 0.1$ and $F_m = 0.4$ and different values of z_G

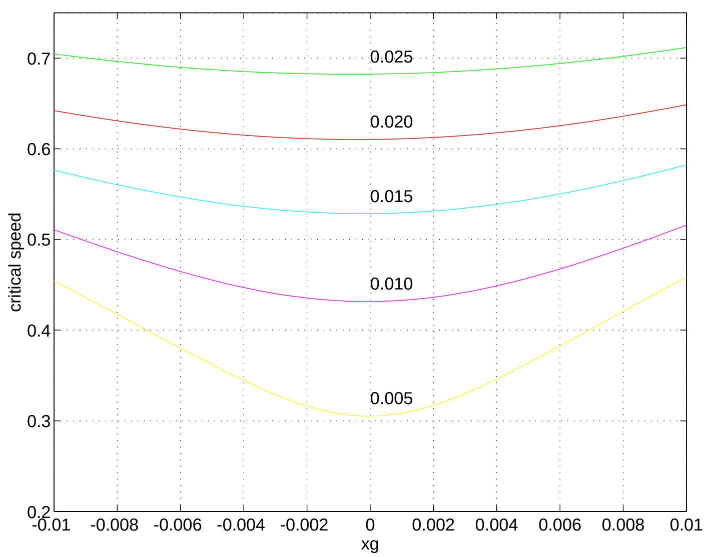

Figure 25: Critical speed versus x_G for $F_n = 0.1$ and $F_m = 0.6$ and different values of z_G

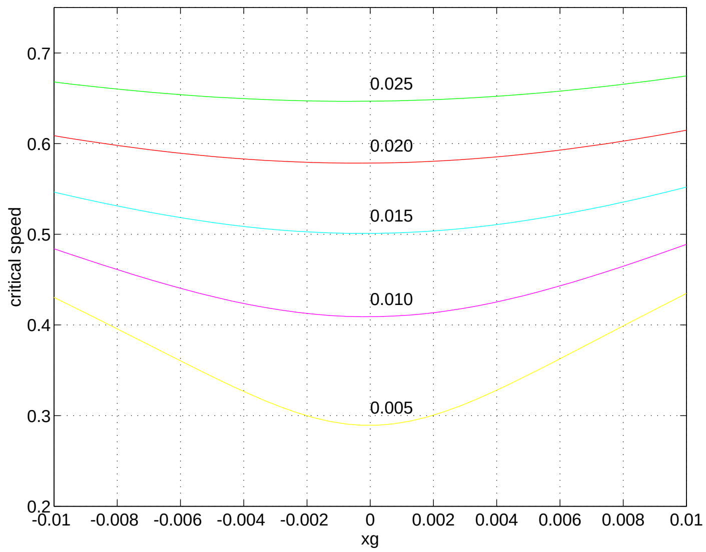

Figure 26: Critical speed versus x_G for $F_n = 0.3$ and $F_m = 0.4$ and different values of z_G

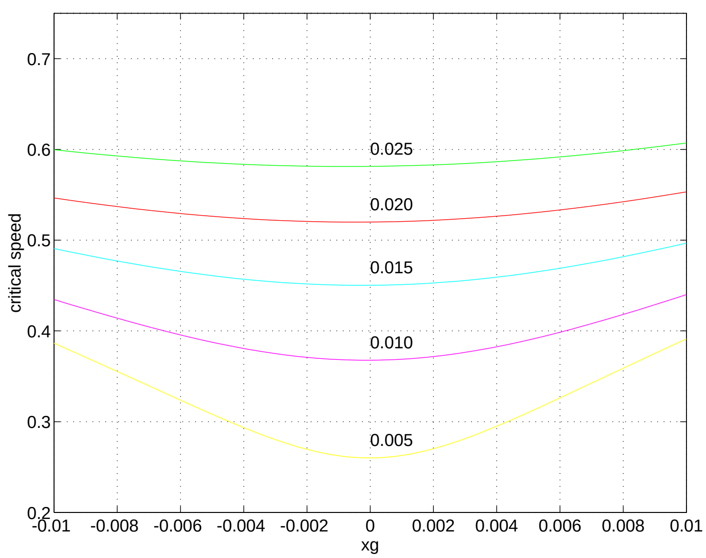

Figure 27: Critical speed versus x_G for $F_n = 0.3$ and $F_m = 0.6$ and different values of z_G

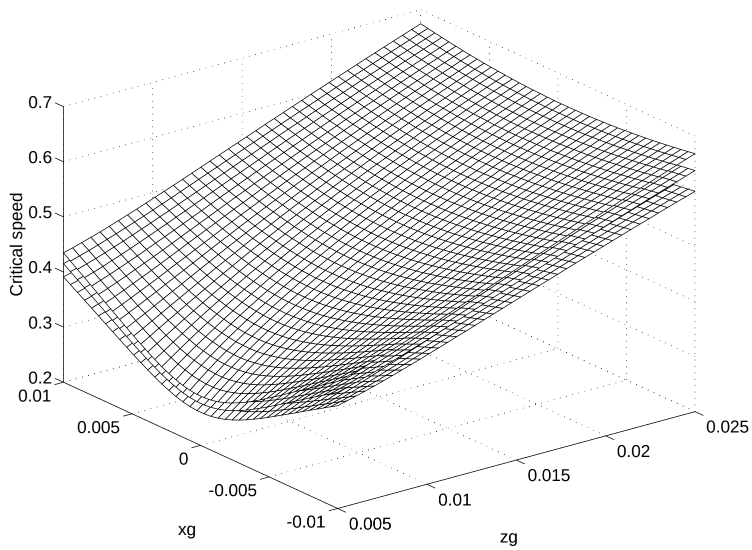

Figure 28: Critical speed versus x_G and z_G for $F_n = 0.3$ and $F_m = 0.4, 0.5, 0.6$

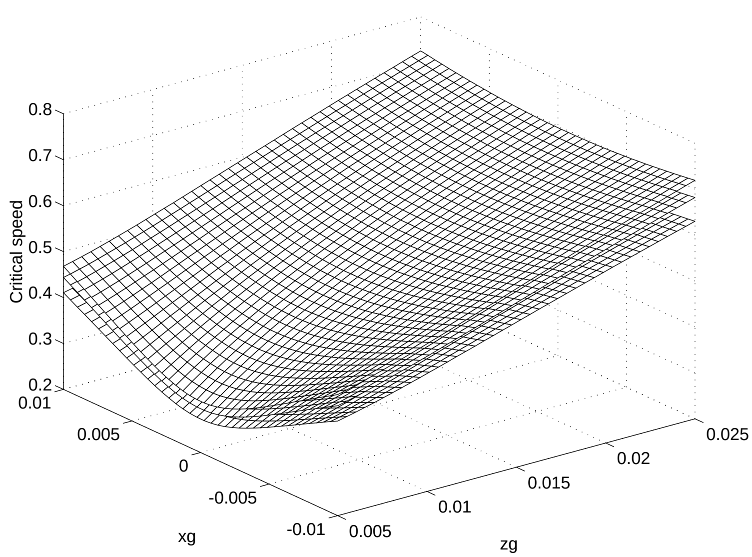

Figure 29: Critical speed versus x_G and z_G for $F_m = 0.5$ and $F_n = 0.1, 0.2, 0.3$

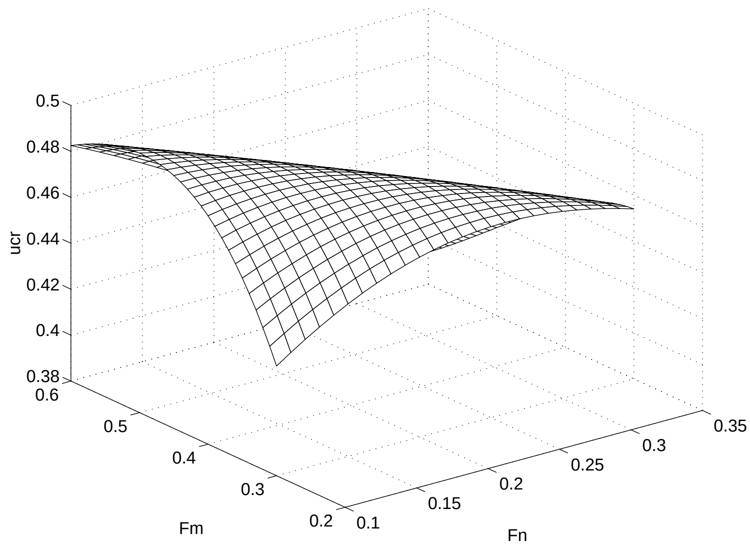

Figure 30: Critical speed versus F_n and F_m for $z_G = 0.0125$ and $x_G = 0$

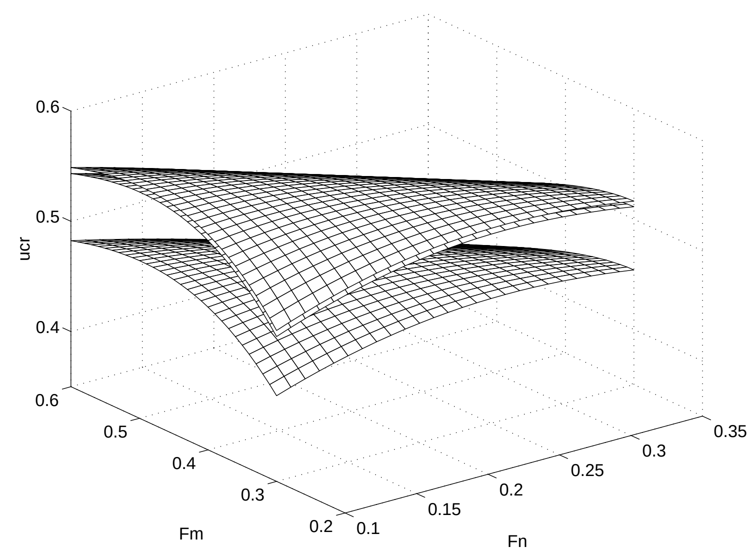

Figure 31: Critical speed versus F_n and F_m for $z_G = 0.0125$ and $x_G = -0.01, 0, +0.01$

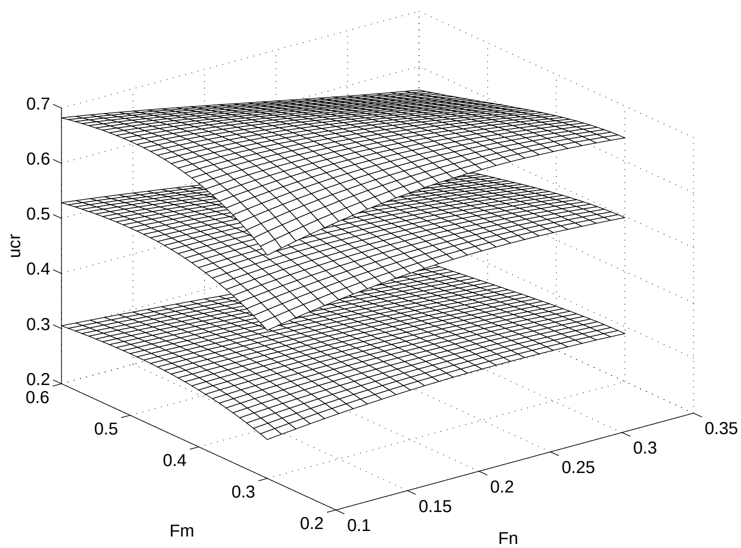

Figure 32: Critical speed versus F_n and F_m for $x_G = 0$ and $z_G = 0.005, 0.015, 0.025$

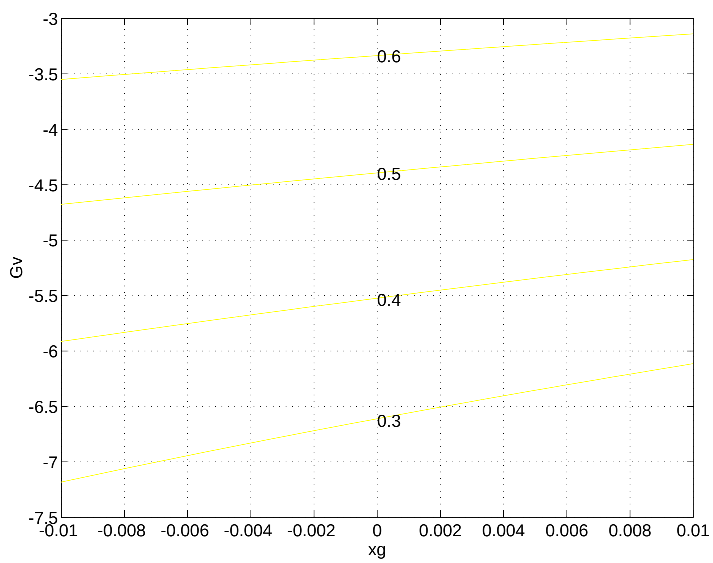

Figure 33: Stability coefficient G_v versus x_G for constant F_n and different values of F_m

using $x_G = -0.01, 0, +0.01$ to plot the surfaces as shown. The lower surface corresponds to $x_G = 0$. It can be seen that nonzero x_G increases the range of stability, while the general trend is to increase stability as both F_n and F_m become smaller. A similar plot for $x_G = 0$ and for three values of z_G, 0.005, 0.010, and 0.025 is shown in Figure 32. The lower surface corresponds to $z_G = 0.005$ and the higher one to $z_G = 0.025$. It can be seen that the metacentric height has by far the greatest effect on dynamic stability, while the effects of hull geometry are smaller.

For comparison, a plot of the classical stability coefficient G_v from equation (1), is shown in Figure 33. The different curves correspond to various mid–body fractions, while the nose fraction is kept constant. It can be seen that G_v is negative throughout. Therefore, it would have predicted an unstable vehicle for all ranges of the parameters, which is of course incorrect. Furthermore, G_v becomes less negative as F_m is increased, which would suggest that dynamic stability is increased as the aft–body length is decreased. This is also a false conclusion. As we pointed out in the introduction, the classical stability index G_v should be used with extreme caution.

III. BIFURCATION ANALYSIS

A. INTRODUCTION

The nonlinear bifurcation analysis is based on the general methodology used in (Papadimitriou, 1994). The fundamental equations are reproduced here for completeness of the presentation. The nonlinear heave/pitch equations of motion (2), (3), and (4) are written in the form,

$$\dot{\theta} = q \; , \tag{7}$$

$$\begin{aligned} \dot{w} &= a_{11}w + a_{12}q + a_{13}(x_{GB}\cos\theta + z_{GB}\sin\theta) \\ &\quad + d_w(w,q) + c_1(w,q) \; , \end{aligned} \tag{8}$$

$$\begin{aligned} \dot{q} &= a_{21}w + a_{22}q + a_{23}(x_{GB}\cos\theta + z_{GB}\sin\theta) \\ &\quad + d_q(w,q) + c_2(w,q) \; , \end{aligned} \tag{9}$$

where the various coefficients are functions of the hydrodynamic derivatives and mass properties, and I_w, I_q are the cross flow integrals.

The system of equations (7) through (9) is written in the compact form

$$\dot{\mathbf{x}} = \mathbf{A}\mathbf{x} + \mathbf{g}(\mathbf{x}) \; , \tag{10}$$

where

$$\mathbf{x} = [\theta, w, q] \; , \tag{11}$$

is the three state variables vector, and $\mathbf{A}$ is the linearized sytem matrix evaluated at the nominal point $\mathbf{x_0}$. The term $\mathbf{g}(\mathbf{x})$ contains all nonlinear terms of the equations. Hopf bifurcation analysis can be performed by isolating the primary nonlinear terms in $\mathbf{g}(\mathbf{x})$. Keeping terms up to third order, we can write

$$\mathbf{g}(\mathbf{x}) = \mathbf{g}^{(2)}(\mathbf{x}) + \mathbf{g}^{(3)}(\mathbf{x}) \; . \tag{12}$$

Using equations (7) through (11), the various terms in (12) can be written as,

$$\begin{aligned} g_1^{(2)} &= 0 \; , \\ g_2^{(2)} &= (I_y - M_{\dot{q}}) m z_G q^2 - (m x_G + Z_{\dot{q}}) m z_G w q \\ &\quad + d_w^{(2)}(w, q) \; , \\ g_3^{(2)} &= -(m - Z_{\dot{w}}) m z_G w q + (m x_G + M_{\dot{w}}) m z_G q^2 \\ &\quad + d_q^{(2)}(w, q) \; , \end{aligned} \tag{13}$$

and

$$\begin{aligned} g_1^{(3)} &= 0 \; , \\ g_2^{(3)} &= d_w^{(3)}(w, q) + \\ &\quad \tfrac{1}{6} a_{13} (x_{GB} \sin\theta_0 - z_{GB} \cos\theta_0) \theta^3 \; , \\ g_3^{(3)} &= d_q^{(3)}(w, q) + \\ &\quad \tfrac{1}{6} a_{23} (x_{GB} \sin\theta_0 - z_{GB} \cos\theta_0) \theta^3 \; . \end{aligned} \tag{14}$$

Expansion in Taylor series of d_w, d_q requires expansion of the cross flow integrals I_w, I_q, which require the Taylor series of

$$f(\xi) = \xi |\xi| \; . \tag{15}$$

This expression can be converted into an analytic function using Dalzell's approximation (Dalzell, (1978),

$$\xi|\xi| \approx \frac{5}{16}\xi_c\xi + \frac{35}{48}\frac{\xi^3}{\xi_c} , \tag{16}$$

which is derived by a least squares fit of an odd series over some assumed range of ξ, namely $-\xi_c < \xi < \xi_c$. This approximation has been extensively used in ship roll motion studies and is very useful for its intended purpose. However, in the present problem it suffers from the several drawbacks (Papadimitriou, 1994). Instead of Dalzell's approximation, we employ the concept of generalized gradient (Clarke, (1983), which is used in the study of control systems involving discontinuous or non–smooth functions. In this way we approximate the gradient of a non–smooth function at a discontinuity by a map equal to the convex closure of the limiting gradients near the discontinuity. In our problem we write,

$$\begin{aligned} f(\xi) \;&=\; \xi_0|\xi_0| + 2|\xi_0|(\xi - \xi_0) + \\ &\qquad \mathrm{sign}(\xi_0)(\xi - \xi_0)^2 + f^{(3)}(\xi) , \end{aligned} \tag{17}$$

as the Taylor series epansion of $f(\xi)$ near ξ_0. The sign function in (17) can be approximated by,

$$\mathrm{sign}(\xi_0) = \lim_{\gamma \to 0} \tanh\left(\frac{\xi_0}{\gamma}\right) . \tag{18}$$

The quantity γ is a small regularization parameter and is used for proper normalization of the results. Using (18), we can approximate $f(\xi)$ in the vicinity of $\xi_0 = 0$ by,

$$\xi|\xi| \approx \frac{1}{6\gamma}\xi^3 . \tag{19}$$

Since

$$\xi \mapsto w - xq \ , \tag{20}$$

we can express the non–smooth cross flow integral terms by,

$$\begin{aligned} I_w &= \frac{C_D}{6\gamma}(E_0 w^3 - 3E_1 w^2 q + 3E_2 w q^2 - E_3 q^3) \ , \\ I_q &= \frac{C_D}{6\gamma}(E_1 w^3 - 3E_2 w^2 q + 3E_3 w q^2 - E_4 q^3) \ , \end{aligned}$$

where

$$E_i = \int_{\text{tail}}^{\text{nose}} x^i b(x)\, dx \ , \tag{21}$$

are the moments of the vehicle "waterplane" area.

Using the previous second and third order Taylor series expansions, equation (10) is written in the form,

$$\dot{\mathbf{x}} = \mathbf{A}\mathbf{x} + \mathbf{g}^{(2)}(\mathbf{x}) + \mathbf{g}^{(3)}(\mathbf{x}) \ . \tag{22}$$

If $\mathbf{T}$ is the matrix of eigenvectors of $\mathbf{A}$ evaluated at the critical point $u = u_c$, the linear change of coordinates,

$$\mathbf{x} = \mathbf{T}\mathbf{z} \ , \quad \mathbf{z} = \mathbf{T}^{-1}\mathbf{x} \ , \tag{23}$$

transforms system (22) into its normal coordinate form,

$$\dot{\mathbf{z}} = \mathbf{T}^{-1}\mathbf{A}\mathbf{T}\mathbf{z} + \mathbf{T}^{-1}\mathbf{g}^{(2)}(\mathbf{T}\mathbf{z}) + \mathbf{T}^{-1}\mathbf{g}^{(3)}(\mathbf{T}\mathbf{z}) \ . \tag{24}$$

At the Hopf bifurcation point, matrix $\mathbf{T}^{-1}\mathbf{A}\mathbf{T}$ takes the form,

$$\mathbf{T}^{-1}\mathbf{A}\mathbf{T} = \begin{bmatrix} 0 & -\omega_0 & 0 \\ \omega_0 & 0 & 0 \\ 0 & 0 & p \end{bmatrix} \ ,$$

where ω_0 is the imaginary part of the critical pair of eigenvalues, and the remaining eigenvalue p is negative. For values of u close to the bifurcation poit u_c, matrix $\mathbf{T}^{-1}\mathbf{A}\mathbf{T}$ becomes,

$$\mathbf{T}^{-1}\mathbf{A}\mathbf{T} = \begin{bmatrix} \alpha'\epsilon & -(\omega_0 + \omega'\epsilon) & 0 \\ (\omega_0 + \omega'\epsilon) & \alpha'\epsilon & 0 \\ 0 & 0 & p + p'\epsilon \end{bmatrix} ,$$

where ϵ denotes the criticality difference

$$\epsilon = u - u_c \ , \tag{25}$$

and

$$\begin{aligned} \alpha' &= \text{derivative of the real part of the critical} \\ &\quad\ \text{eigenvalue with respect to } \epsilon \ , \\ \omega' &= \text{derivative of the imaginary part of the} \\ &\quad\ \text{critical eigenvalue with respect to } \epsilon \ , \\ p' &= \text{derivative of } p \text{ with respect to } \epsilon \ . \end{aligned}$$

Due to continuity, the eigevalue $p + p'\epsilon$ remains negative for small nonzero values of ϵ. Therefore, the coordinate z_3 corresponds to a negative eigenvalue and is asymptotically stable. Center manifold theory predicts that the relationship between the critical coordinates z_1, z_2 and the stable coordinate z_3 is at least of quadratic order. We can then write z_3 as,

$$z_3 = \alpha_{11} z_1^2 + \alpha_{12} z_1 z_2 + \alpha_{22} z_2^2 \ , \tag{26}$$

where the coefficients, α_{ij}, in the quadratic center manifold expansion (26) need to be determined. By differentiating equation (26) we obtain,

$$\dot{z}_3 = 2\alpha_{11} z_1 \dot{z}_1 + \alpha_{12}(\dot{z}_1 z_2 + z_1 \dot{z}_2) + 2\alpha_{22} z_2 \dot{z}_2 \ . \tag{27}$$

We substitute $\dot{z}_1 = -\omega_0 z_2$ and $\dot{z}_2 = \omega_0 z_1$ and we obtain

$$\dot{z}_3 = \alpha_{12}\omega_0 z_1^2 + 2(\alpha_{22} - \alpha_{11})\omega_0 z_1 z_2 - \alpha_{12}\omega_0 z_2^2 \ . \tag{28}$$

The third equation of (24) is written as,

$$\dot{z}_3 = p z_3 + \left[\mathbf{T}^{-1}\mathbf{g}^{(2)}(\mathbf{T}\mathbf{z})\right]_{(3,3)} \ , \tag{29}$$

where terms up to second order have been kept. If we denote the elements of $\mathbf{T}$ and $\mathbf{T}^{-1}$ by,

$$\mathbf{T} = [m_{ij}] \ , \quad \mathbf{T}^{-1} = [n_{ij}] \ , \tag{30}$$

then

$$\mathbf{T}^{-1}\mathbf{g}^{(2)}(\mathbf{T}\mathbf{z}) = \begin{bmatrix} d_1 \\ d_2 \\ d_3 \end{bmatrix} \ ,$$

where expressions for d_1, d_2, d_3, and the coefficients ℓ_{ij} are given in Papadimitriou (1994).

Equation (29) then becomes

$$\dot{z}_3 = p z_3 + d_3 \ , \tag{31}$$

and substituting (26) and the expression for d_3 into (31) we get,

$$\begin{aligned} \dot{z}_3 \quad = \quad & (p\alpha_{11} + n_{32}\ell_{25} + n_{33}\ell_{35}) z_1^2 \\ & +(p\alpha_{12} + n_{32}\ell_{26} + n_{33}\ell_{36}) z_1 z_2 \\ & +(p\alpha_{22} + n_{32}\ell_{27} + n_{33}\ell_{37}) z_2^2 \ . \end{aligned} \tag{32}$$

Comparing coefficients of (28) and (32) we get a system of linear equations which yields the coefficients in the center manifold expansion (26).

Using the previous Taylor expansions and center manifold approximations, we can write the reduced two–dimensional system that describes the center manifold flow of (24) in the form,

$$\begin{aligned}
\dot{z}_1 &= \alpha' \epsilon z_1 - (\omega_0 + \omega' \epsilon) z_2 + F_1(z_1, z_2) \ , \\
\dot{z}_2 &= (\omega_0 + \omega' \epsilon) z_1 + \alpha' \epsilon z_2 + F_2(z_1, z_2) \ ,
\end{aligned}$$

where F_1, F_2 are cubic polynomials in z_1 and z_2.

If we introduce polar coordinates in the form,

$$z_1 = R \cos\phi \ , \quad z_2 = R \sin\phi \ ,$$

we can produce an equation describing the rate of change of the radial coordinate R,

$$\dot{R} = \alpha' \epsilon R + P(\phi) R^3 + Q(\phi) R^2 \ .$$

This equation contains one variable, R, which is slowly varying in time, and another variable, ϕ, which is a fast variable. Therefore, it can be averaged over one complete cycle in ϕ to produce an equation with constant coefficients and similar stability properties,

$$\dot{R} = \alpha' \epsilon R + K R^3 + L R^2 \ ,$$

where

$$K = \frac{1}{2\pi} \int_0^{2\pi} P(\phi) \, d\phi$$

$$
\begin{aligned}
&= \tfrac{1}{8}(3r_{11} + r_{13} + r_{22} + 3r_{24}) \ , \\
L &= \frac{1}{2\pi}\int_0^{2\pi} Q(\phi)\, d\phi = 0 \ .
\end{aligned}
$$

Therefore, the averaged equation becomes

$$\dot{R} = \alpha'\epsilon R + KR^3 \ . \tag{33}$$

Equation (33) admits two steady state solutions, one at $R = 0$ which corresponds to the trivial equilibrium solution at zero, and one at

$$R_0 = \sqrt{-\frac{\alpha'}{K}\epsilon} \ . \tag{34}$$

This equilibrium solution corresponds to a periodic solution or limit cycle in the cartesian coordinates z_1, z_2. For this limit cycle to exist, the quantity R_0 must be a real number. In our case α' is always positive, since the system loses its stability; i.e., the real part of the critical pair of eigenvalues changes from negative to positive, for increasing u. Therefore, existence of these periodic solutions depends on the value of K. Specifically,

- if $K < 0$, periodic solutions exist for $\epsilon > 0$ or $u > u_c$, and
- if $K > 0$, periodic solutions exist for $\epsilon < 0$ or $u < u_c$.

The characteristic root of (33) in the vicinity of (34) is

$$\beta = -2\alpha'\epsilon \ , \tag{35}$$

and we can see that

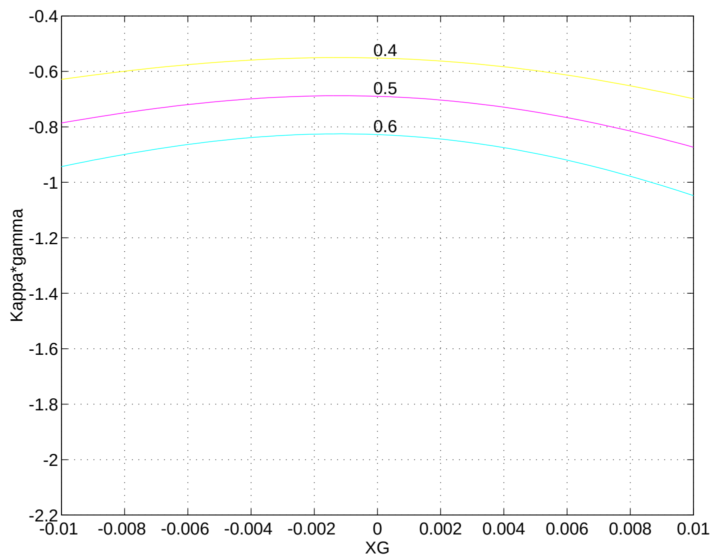

Figure 34: Nonlinear stability coefficient versus x_G for $F_n = 0.1$, $F_m = 0.4$, and different values of C_D

- if periodic solutions exist for $u > u_c$ they are stable, and
- if periodic solutions exist for $u < u_c$ they are unstable.

B. RESULTS AND DISCUSSION

Typical results of the nonlinear stability coefficient K are shown in Figures 34 through 37. Figure 35 presents a plot of $K \cdot \gamma$ versus x_G for $z_G = 0.015$, $F_n = 0.1$, $F_m = 0.6$, and for different values of the quadratic drag coefficient C_D. It should be emphasized that the use of $K \cdot \gamma$ is more meaningful than the use of K, since it properly accounts for the use of the regularization parameter γ. Numerical evidence suggests that all curves $K \cdot \gamma$ versus x_G converge for

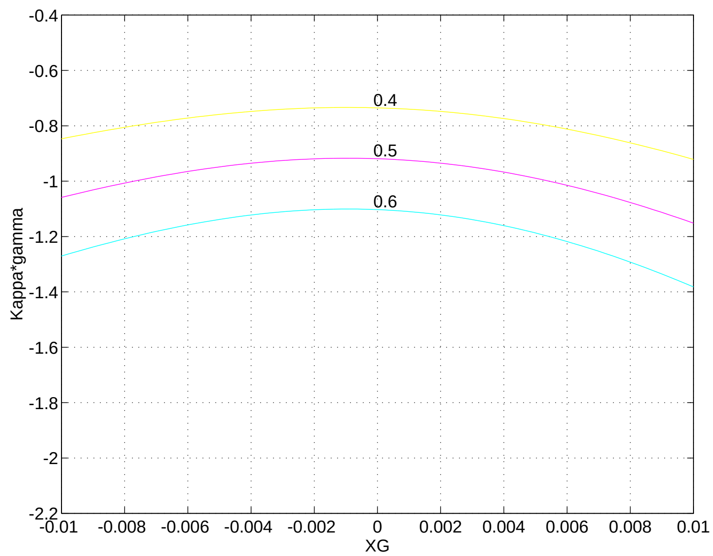

Figure 35: Nonlinear stability coefficient versus x_G for $F_n = 0.1$, $F_m = 0.6$, different values of C_D

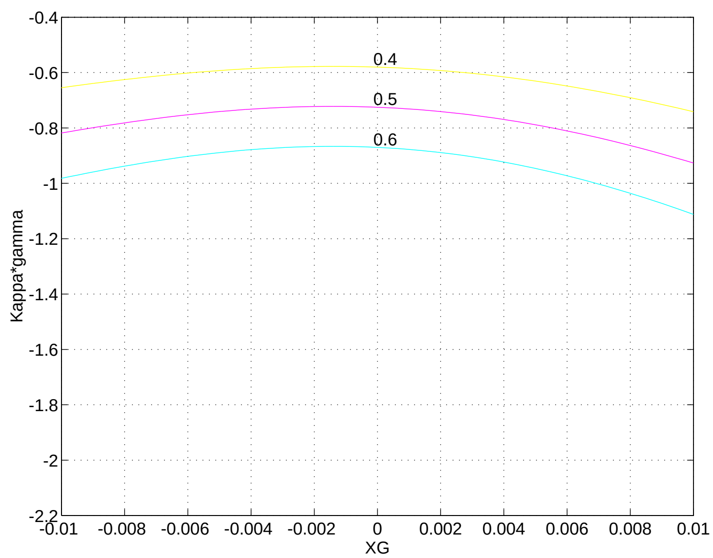

Figure 36: Nonlinear stability coefficient versus x_G for $F_n = 0.3$, $F_m = 0.4$, different values of C_D

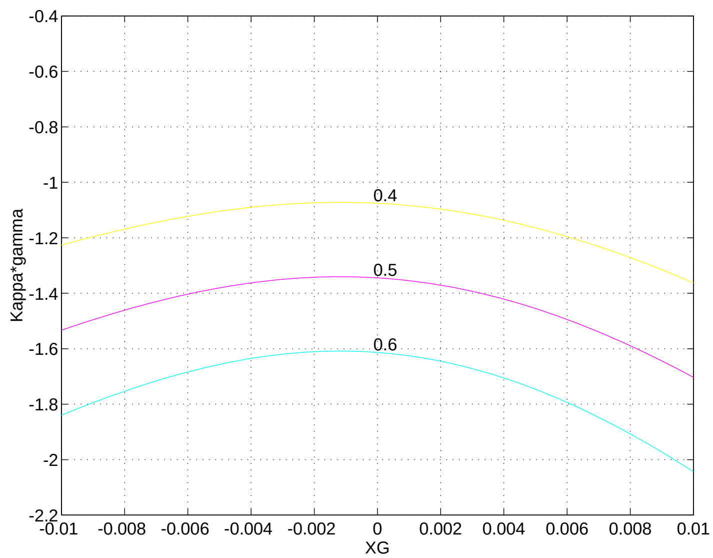

Figure 37: Nonlinear stability coefficient versus x_G for $F_n = 0.3$, $F_m = 0.6$, different values of C_D

$\gamma \rightarrow 0$. For practical purposes, values of γ smaller than 0.001 produce identical results. The results of Figure 8 demonstrate the profound effect that the quadratic drag coefficient C_D has on stability of limit cycles. All Hopf bifurcations are supercritical ($K < 0$), and they become stronger supercritical as C_D is increased. It is worth noting that results for $C_D = 0$ produce subcritical behavior, $K > 0$, which is clearly incorrect. Thus, neglecting the effects of C_D would have produce entirely wrong results in the present problem. Additional results show that the bifurcations become stronger supercritical as initial stability z_G is increased. Figure 34 presents similar results with the only difference being the value of mid–body fraction $F_m = 0.4$. It can be seen that smaller F_m for the same F_n, which results in longer body tail, may be beneficial for stability in the linear sense but it also generates less supercritical bifurcations.

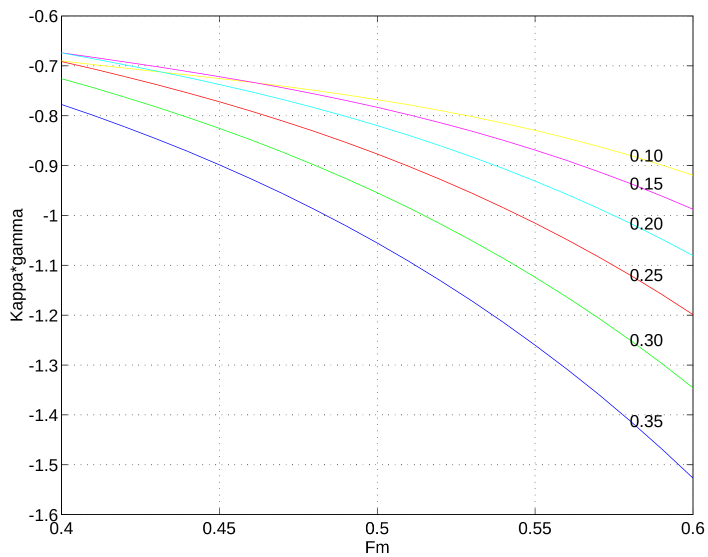

Figure 38: Nonlinear stability coefficient versus F_m for $x_G = 0$, $C_D = 0.5$, and different values of F_n

This can probably be attributed to the increased responsiveness of the vehicle. Figures 36 and 37 show the same results for nose fraction $F_n = 0.3$. It should be emphasized, however, that altering the fore and aft body lengths might infuence the values of C_D which, as we pointed out, is the single most important parameter for the nonlinear nature of the bifurcations.

Figure 38 shows the nonlinear stability coefficient versus F_m for different values of F_n, while $x_G = 0$ and $C_D = 0.5$. It can be seen that smaller F_n for the same F_m, which results in longer body tail, generates less supercritical bifurcations.

Figure 39 shows tne nonlinear stability coefficient versus F_n for different values of F_m, while $x_G = 0$ and $C_D = 0.5$. Again it is clear that longer body

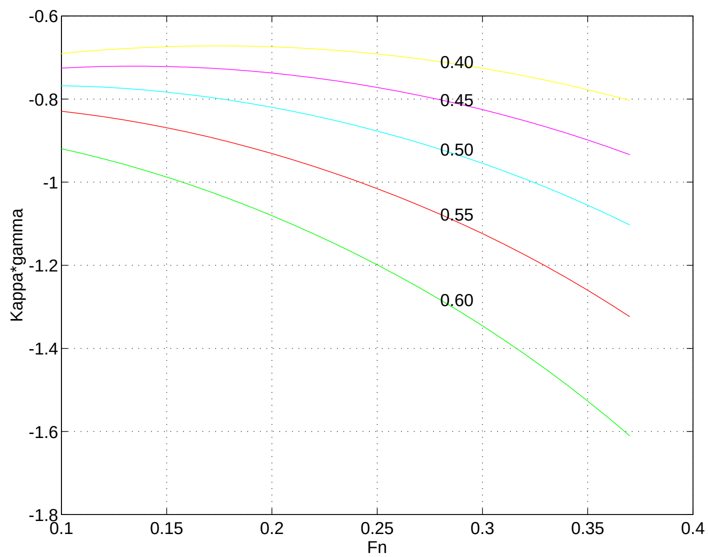

Figure 39: Nonlinear stability coefficient versus F_n for $x_G = 0$, $C_D = 0.5$, and different values of F_m

tail generates less supercritical bifurcations.

IV. CONCLUSIONS AND RECOMMENDATIONS

This work presented a comprehensive nonlinear study of straight line stability of motion of submersibles in the dive plane under open loop conditions. A systematic perturbation analysis demonstrated that the effects of surge in heave/pitch are small and can be neglected. Primary loss of stability was shown to occur in the form of Hopf bifurcations to periodic solutions. The critical speed were instability occurs was computed in terms of metacentric height, longitudinal separation of the centers of buoyancy and gravity, and the dive plane angle. Analysis of the periodic solutions that resulted from the Hopf bifurcations was accomplished through Taylor expansions, up to third order, of the equations of motion. A consistent approximation, utilizing the generalized gradient, was used to study the non–analytic quadratic cross flow integral drag terms. The main results of this study are summarized below:

1. The critical speed of loss of stability is a monotonically increasing function of both vertical and longitudinal LCG/LCB separation. This means that a vehicle which is stable when properly trimmed will remain stable for off–trim conditions.

2. Loss of stability occurs always in the form of supercritical Hopf bifurcations with the generation of stable limit cycles. It was found that this is mainly due to the stabilizing effects of the quadratic drag forces.

3. Even though the quadratic drag forces do not influence the initial loss of stability, they have a significant effect on post–loss of stability stabilization.

4. In general, longer aft body sections seemed to increase the range of linear stability but influence adversely the resulting limit cycles upon the initial loss of stability.

It should be emphasized that the occurrence of supercritical Hopf bifurcations is an attribute of the open loop system only. Under closed loop control, it is possible to experience either supercritical or strongly subcritical Hopf bifurcations, as shown in [Papoulias *et al* (1995)]. The latter are particularly severe in practice since self–sustained vehicle oscillations may be initiated prior to loss of stability, depending on the level of external excitation or the initial conditions.

APPENDIX

The following is a list and description of the computer programs used in this thesis. The programs are written in FORTRAN or MATLAB. Complete print-outs of the programs follow after the list.

- **CRIT_0.M**

  MATLAB program for calculating the critical speed for $\delta = 0$.

- **DSTAB.M**

  MATLAB program for calculating the degree of stability.

- **HOPF_0.FOR**

  FORTRAN program for evaluation of hopf bifurcation formulas using the suboff submarine model.

```
% Program crit_0.m
% Evaluation of critical speed for delta=0

clear
rho = 1.94;
g    = 32.2;
L    = 13.9792;
nd1 = 0.5*rho*L^2;
nd2 = 0.5*rho*L^3;
nd3 = 0.5*rho*L^4;
nd4 = 0.5*rho*L^5;
m   =  1556.2363/(g*nd2);
md  = 1556.2363/g;
V    =  md/rho;

zg    = 0.005;

while zg<0.026,
 flag1    = 0;
 for Fn  = 0.1:0.01:0.35;
  flag1   = flag1+1;
  flag2   = 0;

  for Fm  = 0.3:0.01:0.6;
   flag2   = flag2+1;
   Fb       = 1-Fn-Fm;
   d         = ((12*V)./(pi*L*(3*Fm+2*Fn+Fb))).^0.5;
   r          = d/2;
   Vn     = (2/3*pi*r.^2*L.*Fn);
   Mn     = Vn*rho;
   Vm    = (pi*r.^2.*Fm*L);
   Mm    = Vm*rho;
   Vb     = (1/3*pi*r.^2*L.*Fb);
   Mb     = Vb*rho;
   In      = Mn.*(1/5*(r.^2+(L*Fn).^2)-(3*L*Fn/8).^2);
   Im     = Mm/12.*(3*r.^2+(L*Fm).^2);
   Ib      = Mb.*(3/5*(r.^2/4+(L*Fb).^2)-(L*Fb/4).^2);
   xcb    = pi*d.^2.*(2*L*Fn.*(L*Fm/2+3*L*Fn/8)...
                -L*Fb.*(L*Fb/4+L*Fm/2))/(12*V);
   Lcb    = L*(Fn+Fm/2)-xcb;
   Iyd     = In+Im+Ib+(Mn.*(Lcb-5*L*Fn/8).^2)...
               +(Mm.*(Lcb-L*Fm/2-L*Fn).^2)...
```

```
                +(Mb.*(Lcb-L*(Fn+Fm+Fb/4)).^2);
   Iym    = Iyd/nd4;

% inputs A1,A2,A3,A4,A5,A6,A7,A8 for each coefficient
A1=[-0.0641, 0.0277, -0.0314, -0.0003,  0.0002, -0.0002, -0.0031];
A2=[-0.1149, 0.0499, -0.0559,  0.0040,  0.0007, -0.0007, -0.0046];
A3=[-0.0632, 0.0266, -0.0292,  0.0027,  0.0007, -0.0007, -0.0021];
A4=[ 0.0670,-0.0283,  0.0310, -0.0012, -0.0008,  0.0008,  0.0031];
A5=[ 0.0732,-0.0301,  0.0316, -0.0045, -0.0016,  0.0016,  0.0024];
A6=[-0.0263,-0.0056, -0.0091,  0.0006, -0.0144,  0.0144, -0.0013];
A7=[-0.5769,-1.6357, -0.0880, -0.1590, -1.8067,  1.8067, -0.0808];


% Hydrodynamic coefficient prediction equation
       C1  =  8.023e-3;
       for i = 1:7,
       HCm(i) = A1(i)*Fn.^2+A2(i)*Fn.*Fm...
                       +A3(i)*Fm.^2+A4(i)*Fn...
                      +A5(i)*Fm+A6(i)+A7(i)*(V/L^3-C1);
       end

   zqdot      = -6.33e-4;
   HCm(8) = zqdot;
   ratio  = [0.5686,-1.4357,-0.2658,0.2675,1.1781,-30.5114,0.8149,1.0];
   HC     =  HCm./ratio;

   zqdot   = -6.33e-4;
   zwdot  = HC(5);
   zq       = HC(3);
   zw      = HC(1);
   mqdot  = HC(7);
   mwdot  = HC(6);
   mq      = HC(4);
   mw     = HC(2);
   Iratio   = 0.92943;
   Iy       = Iym/Iratio;
   cd      = 0.015;
   zb      = 0/L;
   xudot  = -0.05*m;
   xb      = 0/L;
   xg      = 0;
```

```
   Gv     = 1 - mw.*(zq+m)./(zw.*(mq-m.*xg));

   xgb    =  xg-xb;
   zgb    =  zg-zb;

    for j = 1:length(zg)
     for i = 1:length(xg)

     theta(i,j) = atan(-xgb(i)./zgb(j));

     a0 = (m-zwdot)*(Iy-mqdot)-(mwdot+m*xg(i))*(zqdot+m*xg(i));
     b0 = (-zwdot*m-m*mw-zq*m)*xg(i)+(-m*mq+zwdot*mq-zqdot*mw...
            -zq*mwdot-m*mwdot-Iy*zw+mqdot*zw);
     c0 = -m*zw*xg(i)+mq*zw-zq*mw-m*mw;
     c1 = (-m*xg(i)+zwdot*xg(i)+m*xb-zwdot*xb)*sin(theta(i,j))...
           +(-m*zb-zwdot*zg(j)+zwdot*zb+m*zg(j))*cos(theta(i,j));
     d1 = (zw*xg(i)-zw*xb)*sin(theta(i,j))...
            +(zw*zb-zw*zg(j))*cos(theta(i,j));

     w(i,j)  = b0*c0/(a0*d1-b0*c1);
     u0(i,j) = (1556.2363/(nd1*w(i,j)))^.5;

     ucr(flag2,flag1) = u0(i,j);

     end
    end

  end
 end

 Fn  = 0.1:0.01:0.35;
 Fm  = 0.3:0.01:0.6;

 mesh(Fn,Fm,ucr/8),grid
 xlabel('Fn')
 ylabel('Fm')
 zlabel('ucr')
 hold on

 zg=zg+0.01;

end
```

```
% Program dstab.m
% Matlab program for calculation the degree of stability

clear
clear global
rho  = 1.94;
g     = 32.2;
L     = 13.9792;
nd1  = 0.5*rho*L^2;
nd2  = 0.5*rho*L^3;
nd3  = 0.5*rho*L^4;
nd4  = 0.5*rho*L^5;
m     = 1556.2363/(g*nd2);
md   = 1556.2363/g;
V     = md/rho;
fig    = 1;
for Fn = 0.1:0.2:0.3,
 for Fm = 0.4:0.2:0.6,
 Fb  = 1-Fn-Fm;
 d     = ((12*V)./(pi*L*(3*Fm+2*Fn+Fb))).^0.5;
 r     = d/2;
 Vn  = (2/3*pi*r.^2*L.*Fn);
 Mn  = Vn*rho;
 Vm  = (pi*r.^2.*Fm*L);
 Mm  = Vm*rho;
 Vb  = (1/3*pi*r.^2*L.*Fb);
 Mb  = Vb*rho;
 In  = Mn.*(1/5*(r.^2+(L*Fn).^2)-(3*L*Fn/8).^2);
 Im  = Mm/12.*(3*r.^2+(L*Fm).^2);
 Ib  = Mb.*(3/5*(r.^2/4+(L*Fb).^2)-(L*Fb/4).^2);
 xcb = pi*d.^2.*(2*L*Fn.*(L*Fm/2+3*L*Fn/8)...
       -L*Fb.*(L*Fb/4+L*Fm/2))/(12*V);
 Lcb = L*(Fn+Fm/2)-xcb;
 Iyd = In+Im+Ib+(Mn.*(Lcb-5*L*Fn/8).^2)...
       +(Mm.*(Lcb-L*Fm/2-L*Fn).^2)...
       +(Mb.*(Lcb-L*(Fn+Fm+Fb/4)).^2);
```

```
 Iym  = Iyd/nd4;


% inputs A1,A2,A3,A4,A5,A6,A7,A8 for each coefficient
A1=[-0.0641, 0.0277, -0.0314, -0.0003,  0.0002, -0.0002, -0.0031];
A2=[-0.1149, 0.0499, -0.0559,  0.0040,  0.0007, -0.0007, -0.0046];
A3=[-0.0632, 0.0266, -0.0292,  0.0027,  0.0007, -0.0007, -0.0021];
A4=[ 0.0670,-0.0283,  0.0310, -0.0012, -0.0008,  0.0008,  0.0031];
A5=[ 0.0732,-0.0301,  0.0316, -0.0045, -0.0016,  0.0016,  0.0024];
A6=[-0.0263,-0.0056, -0.0091,  0.0006, -0.0144,  0.0144, -0.0013];
A7=[-0.5769,-1.6357, -0.0880, -0.1590, -1.8067,  1.8067, -0.0808];


% Hydrodynamic coefficient prediction equation
 C1 = 8.023e-3;
 for i=1:7,
  HCm(i)=A1(i)*Fn.^2+A2(i)*Fn.*Fm+A3(i)*Fm.^2+A4(i)*Fn...
         +A5(i)*Fm+A6(i)+A7(i)*(V/L^3-C1);
 end

 zqdot = -6.33e-4;
 HCm(8) = zqdot;
 ratio = [0.5686,-1.4357,-0.2658,0.2675,1.1781,-30.5114,0.8149,1.0];
 HC=HCm./ratio;

 zqdot  = -6.33e-4;
 zwdot  = HC(5);
 zq     = HC(3);
 zw     = HC(1);
 mqdot  = HC(7);
 mwdot  = HC(6);
 mq     = HC(4);
 mw     = HC(2);
 Iratio = 0.92943;
 iy     = Iym/Iratio;
 cd     = 0.015;
```

```
zg      = 0.015;
zb      = 0/L;
m       = 1556.2363/(g*nd2);
xudot   = -0.05*m;
xb      = 0/L;

xg      = linspace(-0.01,0.01,41);
uo      = 8*linspace(0.2,.6,41);
Gv      = 1 - mw.*(zq+m)./(zw.*(mq-m.*xg));

w       = 1556.2363./(nd1.*uo.^2);
b       = w;
xgb     = xg-xb;
zgb     = zg-zb;
theta   = atan(-xgb./zgb);
for j   = 1:length(uo)
 for i = 1:length(xg)
  A     = [-2*cd  0      0           0;
          0    zw     (zq+m)      0;
          0    mw  (mq-m*xg(i))  (xgb(i)*sin(theta(i))...
                                 -zgb*cos(theta(i)))*b(j);
          0     0      1           0];

  B     = [m-xudot  0                m*zg             0;
          0        m-zwdot      -(m*xg(i)+zqdot)    0;
          m*zg    -(mwdot+m*xg(i))  iy-mqdot        0;
          0        0                0               1];

  evals1 = eig(A,B);  % no surge coupling
  degstab1(i,j) = max(real(evals1));
  end
 end

 figure(fig)
 mesh(uo/8,xg,degstab1),grid
 xlabel('uo')
```

```
  ylabel('xg')
  zlabel('degree of stability')
  fig=fig+1;
 end
end
```

```
C     PROGRAM HOPF.FOR
C     EVALUATION OF HOPF BIFURCATION FORMULAS
C    USING THE SUBOFF SUBMARINE MODEL

C     Cd=0.5, ZG=0.015 ,Fn=0.24, Fm=0.52

      IMPLICIT DOUBLE PRECISION (A-H,O-Z)
      DOUBLE PRECISION L,IY,MASS,MQDOT,MWDOT,ND1,
     1                 MQ,MW,K1,K2,
     2                 BETA,GAMA,
     3                 E0,E1,E2,E3,E4,
     4                 DW1,DW2,DW3,DW4,
     5                 DQ1,DQ2,DQ3,DQ4,
     6                 MASSM,MASSN,MASSB,IB,IM,IN,
     7                 RHO,CD,RADI,VOLM,VOLN,VOLB,LCB,XCB

      DOUBLE PRECISION M11,M12,M13,M21,M22,M23,
     1                 M31,M32,M33,
     2                 N11,N12,N13,N21,N22,N23,
     3                 N31,N32,N33,
     4                 L21,L22,L23,L24,L31,L32,L33,L34,
     5                 L25,L26,L27,L35,L36,L37,
     6                 L21A,L22A,L23A,L24A,L31A,
     7                 L32A,L33A,L34A
      DOUBLE PRECISION LN,LM,LB,FM,FN,FB,KK
C
      DIMENSION A(3,3),T(3,3),TINV(3,3),FV1(3),IV1(3),YYY(3,3)
      DIMENSION WR(3),WI(3),TSAVE(3,3),TLUD(3,3),IVLUD(3)
      DIMENSION ASAVE(3,3),A2(3,3),XL(55),BR(55)
      DIMENSION VEC0(55),VEC1(55),VEC2(55),VEC3(55),VEC4(55)
      DIMENSION HCA1(7),HCA2(7),HCA3(7),HCA4(7),HCA5(7)
      DIMENSION HCA6(7),HCA7(7),HC(8),RATIO(7),SVLUD(3)

C
      OPEN (20,FILE='DATA_0.DAT',STATUS='NEW')
C
```

```
      WEIGHT= 1556.2363
      L     =   13.9792
      RHO   =    1.94
      DO 8886 CD1  =  0.40,0.60,0.10
      CD    =  0.5*CD1*RHO
      G     =  32.2
      XB    =   0.0
      DO 8887 KK = 0.0050,0.0250,0.0050
      ZG    = KK*L
      ZB    =   0.0
      MASS  = WEIGHT/G
      BOY   = WEIGHT
      VOLUME= MASS/RHO
      DO 8888 FN=0.10,0.32,0.10
      DO 8889 FM=0.40,0.62,0.10

C      WRITE (20,*) 'CD =',CD
C      WRITE (20,*) 'ZG =',KK
C      WRITE (20,*) 'FN =',FN
C      WRITE (20,*) 'FM =',FM

      FB      = 1.0-FN-FM
      LN      = L*FN
      LM     = L*FM
      LB       = L*FB
      DIAM  = SQRT((12.*VOLUME)
     &                       /(3.14159*L*(3.*FM+2.*FN+FB)))
      WRITE(*,4001) DIAM
      RADI      = DIAM/2.
      VOLN     = (2./3.*3.14159*RADI**2.*L*FN)
      MASSN  = VOLN*RHO
      VOLM   = (3.14159*RADI**2.*FM*L)
      MASSM = VOLM*RHO
      VOLB     = (1./3.*3.14159*RADI**2.*L*FB)
      MASSB  = VOLB*RHO
      IN          = MASSN*(1./5.*(RADI**2+(L*FN)**2)
```

```
     &                  -(3*L*FN/8)**2)
      IM          = MASSM/12.*(3.*RADI**2.+(L*FM)**2)
      IB           = MASSB*(3./5.*(RADI**2/4.
     &                  +(L*FB)**2)-(L*FB/4.)**2)
      XCB       = (3.14159*DIAM**2*(2.*L*FN
     &                *(L*FM/2.+3.*L*FN/8.)
     &                -L*FB*(L*FB/4.+L*FM/2.)))/(12.*VOLUME)
      WRITE(*,4001) XCB
      LCB       = L*(FN+FM/2.)-XCB
      WRITE(*,4001) LCB
      IY         = IN+IM+IB+MASSN*(LCB-5*L*FN/8)**2
    &              +MASSM*(LCB-L*FM/2-L*FN)**2
      IY = IY+MASSB*(LCB-L*(FN+FM+FB/4))**2

C     Inputs A1,A2,A3,A4,A5,A6,A7,A8 for each coefficient

      HCA1(1)  = -0.0641
      HCA1(2)  =  0.0277
      HCA1(3)  = -0.0314
      HCA1(4)  = -0.0003
      HCA1(5)  =  0.0002
      HCA1(6)  = -0.0002
      HCA1(7)  = -0.0031
      HCA2(1)  = -0.1149
      HCA2(2)  =  0.0499
      HCA2(3)  = -0.0559
      HCA2(4)  =  0.0040
      HCA2(5)  =  0.0007
      HCA2(6)  = -0.0007
      HCA2(7)  = -0.0046
      HCA3(1)  = -0.0632
      HCA3(2)  =  0.0266
      HCA3(3)  = -0.0292
      HCA3(4)  =  0.0027
      HCA3(5)  =  0.0007
      HCA3(6)  = -0.0007
```

```
      HCA3(7)  = -0.0021
      HCA4(1)  =  0.0670
      HCA4(2)  = -0.0283
      HCA4(3)  =  0.0310
      HCA4(4)  = -0.0012
      HCA4(5)  = -0.0008
      HCA4(6)  =  0.0008
      HCA4(7)  =  0.0031
      HCA5(1)  =  0.0732
      HCA5(2)  = -0.0301
      HCA5(3)  =  0.0316
      HCA5(4)  = -0.0045
      HCA5(5)  = -0.0016
      HCA5(6)  =  0.0016
      HCA5(7)  =  0.0024
      HCA6(1)  = -0.0263
      HCA6(2)  = -0.0056
      HCA6(3)  = -0.0091
      HCA6(4)  =  0.0006
      HCA6(5)  = -0.0144
      HCA6(6)  =  0.0144
      HCA6(7)  = -0.0013
      HCA7(1)  = -0.5796
      HCA7(2)  = -1.6357
      HCA7(3)  = -0.0880
      HCA7(4)  = -0.1590
      HCA7(5)  = -1.8067
      HCA7(6)  =  1.8067
      HCA7(7)  = -0.0808

C      Hydrodynamic coefficient prediction equation
C
      C1              =  8.023E-03
      RATIO(1)  =   0.5686
      RATIO(2)  =  -1.4357
      RATIO(3)  =   -0.2658
```

```
      RATIO(4)  =    0.2675
      RATIO(5)  =    1.1781
      RATIO(6)  = -30.5114
      RATIO(7)  =    0.8149

      DO 5000 I=1,7
       HC(I)=(HCA1(I)*FN**2+HCA2(I)*FN*FM
     &          +HCA3(I)*FM**2+HCA4(I)*FN
     &          +HCA5(I)*FM+HCA6(I)
     &          +HCA7(I)*(VOLUME/(L*L*L)-C1))/RATIO(I)

 5000 CONTINUE

      HC(8)    =  -6.33E-04
      ZQDOT      =  -6.33E-04*0.5*RHO*L**4
      HC(8)          =   ZQDOT
      ZWDOT     =   HC(5)*0.5*RHO*L**3
      ZQ              =   HC(3)*0.5*RHO*L**3
      ZW             =   HC(1)*0.5*RHO*L**2
      MQDOT     = HC(7)*0.5*RHO*L**5
      MWDOT    = HC(6)*0.5*RHO*L**4
      MQ             = HC(4)*0.5*RHO*L**4
      MW            = HC(2)*0.5*RHO*L**3
      RATIO1      =  0.92943
      IY                 =  IY/RATIO1
      WRITE(*,4001) IY
      ND1           = 0.5*RHO*L**2
      ZGB           =  ZG-ZB
C
C     DEFINE THE LENGTH X AND BREADTH B TERMS FOR THE INTEGRATION
C

      DO 333 I=0,21
       XL(I+1)= I*LB/21.0
       BR(I+1)=DIAM*XL(I+1)/LB
  333 CONTINUE
```

```
      DO 334 I=1,2
       XL(22+I)= LB+I*LM/2.0
       BR(22+I)=DIAM
  334 CONTINUE
      DO 335 I=1,30
c       WRITE(*,*) I
       XL(I+24)= XL(I+23)+1./4.*(L-XL(I+23))
       IF  (((XL(I+24)-LB-LM)**2/(LN**2)).GT.1.0) THEN
        BR(I+24)=0.0
       ELSE
        BR(I+24)=DIAM*SQRT(1.0-((XL(I+24)-LB-LM)**2/(LN**2)))
       ENDIF
  335 CONTINUE
       XL(55) = L
       BR(55) = 0
      DO 102 N = 1,55
        XL(N) = XL(N)-L+LCB
 102  CONTINUE

      WRITE(20,7001) XL
      WRITE(20,7001) BR
C
      DO 104 K = 1,55
        VEC0(K)=BR(K)
        VEC1(K)=XL(K)*BR(K)
        VEC2(K)=XL(K)*XL(K)*BR(K)
        VEC3(K)=XL(K)*XL(K)*XL(K)*BR(K)
        VEC4(K)=XL(K)*XL(K)*XL(K)*XL(K)*BR(K)
  104 CONTINUE
      CALL TRAP(55,VEC0,XL,E0)
      CALL TRAP(55,VEC1,XL,E1)
      CALL TRAP(55,VEC2,XL,E2)
      CALL TRAP(55,VEC3,XL,E3)
      CALL TRAP(55,VEC4,XL,E4)

      EPSILON = 0.001
```

```
      XGMIN=-0.01
      XGMAX=+0.01
      IXG=80
      XGMIN=XGMIN*L
      XGMAX=XGMAX*L

C==================================================================

      DO 1 IT=1,IXG
C        WRITE (*,3001) IT,IXG
        XG=XGMIN+(XGMAX-XGMIN)*(IT-1)/(IXG-1)
        XGB=XG-XB
        DV=(MASS-ZWDOT)*(IY-MQDOT)
      &        -(MASS*XG+ZQDOT)*(MASS*XG+MWDOT)
        CD6=CD/(3.D0*EPSILON*DV)
        DW1=CD6*((IY-MQDOT)*(-E0)+(MASS*XG+ZQDOT)*E1)
        DW2=CD6*((IY-MQDOT)*(3*E1)-(MASS*XG+ZQDOT)*3*E2)
        DW3=CD6*((IY-MQDOT)*(-3*E2)+(MASS*XG+ZQDOT)*3*E3)
        DW4=CD6*((IY-MQDOT)*(E3)-(MASS*XG+ZQDOT)*E4)
        DQ1=CD6*((MASS-ZWDOT)*(E1)+(MASS*XG+MWDOT)*(-E0))
        DQ2=CD6*((MASS-ZWDOT)*(-3*E2)+(MASS*XG+MWDOT)*(3*E1))
        DQ3=CD6*((MASS-ZWDOT)*(3*E3)+(MASS*XG+MWDOT)*(-3*E2))
        DQ4=CD6*((MASS-ZWDOT)*(-E4)+(MASS*XG+MWDOT)*(E3))
        THETA0=ATAN(-XGB/ZGB)
        AA0=(MASS-ZWDOT)*(IY-MQDOT)
     &          -(MWDOT+MASS*XG)*(ZQDOT+MASS*XG)
        BB0=(-ZWDOT*MASS-MASS*MW-ZQ*MASS)*XG
     &     +(-MASS*MQ+ZWDOT*MQ-ZQDOT*MW
     &     -ZQ*MWDOT-MASS*MWDOT-IY*ZW+MQDOT*ZW)
        CC0=-MASS*ZW*XG+MQ*ZW-ZQ*MW-MASS*MW
        CC1=(-MASS*XG+ZWDOT*XG+MASS*XB-ZWDOT*XB)*SIN(THETA0)
     &     +(-MASS*ZB-ZWDOT*ZG+ZWDOT*ZB+MASS*ZG)*COS(THETA0)
        DD1=(ZW*XG-ZW*XB)*SIN(THETA0)+(ZW*ZB-ZW*ZG)
     &      *COS(THETA0)

C After applying AD=BC ( Routh Criterion ), we manage to calculate
```

```
C the critical speed U0.

        WEI=BB0*CC0/(AA0*DD1-BB0*CC1)
        U0=DSQRT(1556.2363/WEI)
        U=U0
        WRITE (*,*) U/8.0,XG/L
C
C       DETERMINE [A] AND [B] COEFFICIENTS
C
        A11DV=(IY-MQDOT)*ZW+(MASS*XG+ZQDOT)*MW
        A12DV=(IY-MQDOT)*(MASS+ZQ)+(MASS*XG+ZQDOT)*(MQ-MASS*XG)
        A13DV=-(MASS*XG+ZQDOT)*WEIGHT
        A21DV=(MASS-ZWDOT)*MW+(MASS*XG+MWDOT)*ZW
        A22DV=(MASS-ZWDOT)*(MQ-MASS*XG)+(MASS*XG+MWDOT)*(MASS+ZQ)
        A23DV=-(MASS-ZWDOT)*WEIGHT
C
        A11=A11DV/DV
        A12=A12DV/DV
        A13=A13DV/DV
        A21=A21DV/DV
        A22=A22DV/DV
        A23=A23DV/DV
C
        C11DV=(IY-MQDOT)*MASS*ZG
        C12DV=-(MASS*XG+ZQDOT)*MASS*ZG
        C21DV=-(MASS-ZWDOT)*MASS*ZG
        C22DV=(MASS*XG+MWDOT)*MASS*ZG
C
        C11=C11DV/DV
        C12=C12DV/DV
        C21=C21DV/DV
        C22=C22DV/DV
C==================================================================
C       EVALUATE TRANSFORMATION MATRIX OF EIGENVECTORS
C
        K1=-(XGB*SIN(THETA0)-ZGB*COS(THETA0))
```

```
      K2=-(1./6.)*(ZGB*COS(THETA0)-XGB*SIN(THETA0))
C
      A(1,1)=0.0
      A(1,2)=0.0
      A(1,3)=1.0
      A(2,1)=A13*K1
      A(2,2)=A11*U
      A(2,3)=A12*U
      A(3,1)=A23*K1
      A(3,2)=A21*U
      A(3,3)=A22*U
      DO 11 I=1,3
        DO 12 J=1,3
          ASAVE(I,J)=A(I,J)
   12   CONTINUE
   11 CONTINUE
      CALL RG(3,3,A,WR,WI,1,YYY,IV1,FV1,IERR)
      CALL DSOMEG(IEV,WR,WI,OMEGA,CHECK)
C      WRITE (*,*) IEV
C      WRITE (*,*) (WR(IWR),IWR=1,3)
C      WRITE (*,*) (WI(IWI),IWI=1,3)
      OMEGA0=OMEGA
      DO 5 I=1,3
        T(I,1)= YYY(I,IEV)
        T(I,2)=-YYY(I,IEV+1)
    5 CONTINUE
      IF (IEV.EQ.1) GO TO 13
      IF (IEV.EQ.2) GO TO 14
      STOP 3004
   14 DO 6 I=1,3
        T(I,3)=YYY(I,1)
    6 CONTINUE
      GO TO 17
   13 DO 16 I=1,3
        T(I,3)=YYY(I,3)
   16 CONTINUE
```

```
   17   CONTINUE
C
C       NORMALIZATION OF THE CRITICAL EIGENVECTOR
C
        INORM=1
        IF (INORM.NE.0) CALL NORMAL(T)
C
C       INVERT TRANSFORMATION MATRIX
C
        DO 2 I=1,3
          DO 3 J=1,3
            TINV(I,J)=0.0
            TSAVE(I,J)=T(I,J)
    3     CONTINUE
    2   CONTINUE
        CALL DLUD(3,3,TSAVE,3,TLUD,IVLUD)
        DO 4 I=1,3
          IF (IVLUD(I).EQ.0) STOP 3003
    4   CONTINUE
        CALL DILU(3,3,TLUD,IVLUD,SVLUD)
        DO 8 I=1,3
          DO 9 J=1,3
            TINV(I,J)=TLUD(I,J)
    9     CONTINUE
    8   CONTINUE
C
C       CHECK Inv(T)*A*T
C
        IMULT=1
        IF (IMULT.EQ.1) CALL MULT(TINV,ASAVE,T,A2)
        IF (IMULT.EQ.0) STOP
        P=A2(3,3)
        PEIG=P
C        WRITE (*,4001) (A2(1,JA2),JA2=1,3)
C        WRITE (*,4001) (A2(2,JA2),JA2=1,3)
C        WRITE (*,4001) (A2(3,JA2),JA2=1,3)
```

```
C         PAUSE
C
C        DEFINITION OF Nij
C
         N11=TINV(1,1)
         N21=TINV(2,1)
         N31=TINV(3,1)
         N12=TINV(1,2)
         N22=TINV(2,2)
         N32=TINV(3,2)
         N13=TINV(1,3)
         N23=TINV(2,3)
         N33=TINV(3,3)
C
C        DEFINITION OF Mij
C
         M11=T(1,1)
         M21=T(2,1)
         M31=T(3,1)
         M12=T(1,2)
         M22=T(2,2)
         M32=T(3,2)
         M13=T(1,3)
         M23=T(2,3)
         M33=T(3,3)
C
C        DEFINITION OF Lij
C
         L25=C11*M31*M31+C12*M21*M31
         L26=2*C11*M31*M32+C12*(M21*M32+M22*M31)
         L27=C11*M32*M32+C12*M22*M33
         L35=C22*M31*M31+C21*M21*M31
         L36=2*C22*M31*M32+C21*(M21*M32+M22*M31)
         L37=C22*M32*M32+C21*M33*M22
C
C        DEFINITION OF ALFA, BETA, GAMA
```

```
C
      D1 =N32*L25 + N33*L35
      D2 =N32*L26 + N33*L36
      D3 =N32*L27 + N33*L37
C
      D11=-P
      D12=OMEGA0
      D21=-2*OMEGA0
      D22=-P
      D23=2*OMEGA0
      D32=-OMEGA0
      D33=-P
C
      BETA=(D2-D21*D1/D11-D23*D3/D33)
     &            /(D22-D21*D12/D11-D23*D32/D33)
      ALFA=(D1-D12*BETA)/D11
      GAMA=(D3-D32*BETA)/D33
C
      L21A=2*C11*ALFA*M31*M33+C12*ALFA
    &           *(M21*M33+M23*M31)
C
      L22A=2*C11*ALFA*M32*M33 + 2*C11*BETA*M31*M33
    &      +  C12*ALFA*(M22*M33+M32*M23)
    &      +  C12*BETA*(M21*M33+M23*M31)
C
      L23A=2*C11*GAMA*M31*M33+2*C11*BETA*M32*M33
    &      +  C12*GAMA*(M21*M33+M23*M31)
    &      +  C12*BETA*(M22*M33+M23*M32)
C
      L24A=2*C11*GAMA*M32*M33+C12*GAMA
     &          *(M22*M33+M23*M32)
C
      L31A=2*C22*ALFA*M31*M33+C21*ALFA
     &          *(M21*M33+M23*M31)
C
      L32A=2*C22*ALFA*M32*M33+2*C22*BETA*M31*M33
```

```
     &      +  C21*ALFA*(M22*M33+M32*M23)
     &      +  C21*BETA*(M21*M33+M23*M31)
C
        L33A=2*C22*GAMA*M31*M33+2*C22*BETA*M32*M33
     &      +  C21*GAMA*(M21*M33+M23*M31)
     &      +  C21*BETA*(M22*M33+M23*M32)
C
        L34A=2*C22*GAMA*M32*M33+C21*GAMA
      &          *(M22*M33+M23*M32)
C
        L21=L21A+A13*K2*M11**3+DW1*M21**3
     &             +DW2*M31*M21**2
     &             +DW3*M21*M31**2+DW4*M31**3
        L22=L22A+3*A13*K2*M12*M11**2+3*DW1*M22*M21**2
     &              +DW2*(2*M21*M22*M31+M32*M21**2)
     &              +DW3*(2*M21*M31*M32+M22*M31**2)
     &              +3*DW4*M32*M31**2
        L23=L23A+3*A13*K2*M11*M12**2+3*DW1*M21*M22**2
     &              +DW2*(M31*M22**2+2*M21*M22*M32)
     &     +     DW3*(M21*M32**2+2*M22*M31*M32)
     &     +     3*DW4*M31*M32**2
        L24=L24A+A13*K2*M12**3+DW1*M22**3
     &              +DW2*M32*M22**2
     &             +DW3*M22*M32**2+DW4*M32**3
        L31=L31A+A23*K2*M11**3+DQ1*M21**3
     &              +DQ2*M31*M21**2
     &              +DQ3*M21*M31**2+DQ4*M31**3
        L32=L32A+3*A23*K2*M12*M11**2+3*DQ1*M22*M21**2
     &              +DQ2*(2*M21*M22*M31+M32*M21**2)
     &              +DQ3*(2*M21*M31*M32+M22*M31**2)
     &               +3*DQ4*M32*M31**2
        L33=L33A+3*A23*K2*M11*M12**2+3*DQ1*M21*M22**2
     &     +     DQ2*(M31*M22**2+2*M21*M22*M32)
     &     +     DQ3*(M21*M32**2+2*M22*M31*M32)
     &     +     3*DQ4*M31*M32**2
        L34=L34A+A23*K2*M12**3+DQ1*M22**3
```

```
     &                +DQ2*M32*M22**2
     &                +DQ3*M22*M32**2+DQ4*M32**3
C
      R11=N12*L21+N13*L31
      R12=N12*L22+N13*L32
      R13=N12*L23+N13*L33
      R14=N12*L24+N13*L34
      R21=N22*L21+N23*L31
      R22=N22*L22+N23*L32
      R23=N22*L23+N23*L33
      R24=N22*L24+N23*L34
C
C     EVALUATE DALPHA AND DOMEGA
C
      UINC=0.001
      UR =U+UINC
      UL =U-UINC
      U  =UR
C
      A(1,1)=0.0
      A(1,2)=0.0
      A(1,3)=1.0
      A(2,1)=A13*K1
      A(2,2)=A11*U
      A(2,3)=A12*U
      A(3,1)=A23*K1
      A(3,2)=A21*U
      A(3,3)=A22*U
C
      CALL RG(3,3,A,WR,WI,0,YYY,IV1,FV1,IERR)
      CALL DSTABL(DEOS,WR,WI,FREQ)
      ALPHR=DEOS
      OMEGR=FREQ
C
      U=UL
C
```

```
      A(1,1)=0.0
      A(1,2)=0.0
      A(1,3)=1.0
      A(2,1)=A13*K1
      A(2,2)=A11*U
      A(2,3)=A12*U
      A(3,1)=A23*K1
      A(3,2)=A21*U
      A(3,3)=A22*U
C
      CALL RG(3,3,A,WR,WI,0,YYY,IV1,FV1,IERR)
      CALL DSTABL(DEOS,WR,WI,FREQ)
      ALPHL=DEOS
      OMEGL=FREQ
C
      DALPHA=(ALPHR-ALPHL)/(UR-UL)
      DOMEGA=(OMEGR-OMEGL)/(UR-UL)
C
C     EVALUATION OF HOPF BIFURCATION COEFFICIENTS
C
      COEF1=3.0*R11+R13+R22+3.0*R24
      COEF2=3.0*R21+R23-R12-3.0*R14
      AMU2 =-COEF1/(8.0*DALPHA)
      BETA2=0.25*COEF1
C     TAU2 =-(COEF2-DOMEGA*COEF1/DALPHA)/(8.0*OMEGA0)
C     PER  =2.0*3.1415927/OMEGA0
C     PER  =PER*U/L
C      WRITE (20,2001) XCB
      WRITE (20,2001) XG/L,COEF1
   1  CONTINUE
 8889 CONTINUE
 8888 CONTINUE
 8887 CONTINUE
 8886 CONTINUE
       STOP
 1001 FORMAT (' ENTER NUMBER OF DATA LINES')
```

```
1002 FORMAT (' ENTER UO, ZG, AND DSAT')
1003 FORMAT (' ENTER BOW PLANE TO STERN PLANE RATIO')
1004 FORMAT (' ENTER ZG')
2001 FORMAT (2E14.5)
4001 FORMAT (1F15.5)
7001 FORMAT (6F15.5)
3001 FORMAT (2I5)
     END
```

LIST OF REFERENCES

- Arentzen, E. S. and Mandel, P. [1960] "Naval architectural aspects of submarine design", *Trans. Soc. of Naval Archit. & Marine Engrs.*, **68**, pp. 662–692.
- Bender, C. M. and Orszag, S. A. [1978] *Advanced Mathematical Methods for Scientists and Engineers* (McGraw–Hill, New York).
- Chow, S.–N. and Mallet–Paret, J. [1977] "Integral averaging and bifurcation", *Journal of Differential Equations*, **26**, pp. 112–159.
- Clayton, B. R. and Bishop, R. E. D. [1982] *Mechanics of Marine Vehicles* (Gulf Publishing Company, Houston).
- Clarke, F. [1983] *Optimization and Nonsmooth Analysis* (Wiley and Sons, New York).
- Dalzell, J. F. [1978] "A note on the form of ship roll damping", *Journal of Ship Research*, **22**, 3.
- Feldman, J. [1987] Straightline and rotating arm captive–model experiments to investigate the stability and control characteristics of submarines and other submerged vehicles. Carderock Division, Naval Surface Warfare Center, Report DTRC/SHD–0303–20.
- Fidler J. and Smith C. [1978] Methods for predicting submersible hydrodynamic characteristics. Naval Coastal Systems Center, Report TM–238–78.
- Gertler, M. and Hagen, G. R. [1967] Standard equations of motion for submarine simulation. David Taylor Research Center, Report 2510.
- Guckenheimer, J. and Holmes, P. [1983] *Nonlinear Oscillations, Dynamical Systems, and Bifurcations of Vector Fields* (Springer–Verlag, New York).
- Hassard, B. and Wan, Y.H. [1978] "Bifurcation formulae derived from center manifold theory", *Journal of Mathematical Analysis and Applications*, **63**, pp. 297–312.
- Holmes, E. P. [1995] Prediction of hydrodynamic coefficients utilizing geometric considerations. Master's Thesis, Naval Postgraduate School, Monterey, California.

- Humphreys, D. E. and Watkinson, K. [1978] Prediction of acceleration hydrodynamic coefficients for underwater vehicles from geometric parameters. Naval Coastal Systems Laboratory, Report TR–327–78.

- Papadimitriou, H. I. [1994] A nonlinear study of open loop dynamic stability of submersible vehicles in the dive plane. Master of Science in Mechanical Engineering and Mechanical Engineer's Thesis, Naval Postgraduate School, Monterey, California.

- Papoulias F. A., Aydin, I., and McKinley, B. D. [1993] "Characterization of steady state solutions of submarines under casualty conditions", in *Nonlinear Dynamics of Marine Vehicles* (J. M. Falzarano, F. A. Papoulias, eds.), (ASME, New York).

- Papoulias F. A., Bateman, C. A., and Ornek, S. [1995] "Dynamic loss of stability in depth control of submersible vehicles", *Journal of Applied Ocean Research*, **17**, 6.

- Papoulias, F. A. and Papadimitriou, H. A. [1995] "Nonlinear studies of dynamic stability of submarines in the dive plane", *Journal of Ship Research*, **39**, 4.

- Peterson, R. S. [1980] Evaluation of semi–empirical methods for predicting linear static and rotary hydrodynamic coefficients. Naval Coastal Systems Center, Report TM–291–80.

- Roddy, R. F. [1990] Investigation of the stability and control characteristics of several configurations of the DARPS SUBOFF model (DTRC model 5470) from captive–model experiments. Carderock Division, Naval Surface Warfare Center, Report DTRC/SHD–1298–08.

- Smith, N. S., Crane, J. W., and Summey, D. C. [1978] SDV simulator hydrodynamic coefficients. Naval Coastal Systems Center, Report NCSC–TM231–78.

- Tinker, S. J. [1978] "Fluid memory effects on the trajectory of a submersible", *International Shipbuilding Progress*, **25**, 290.

- Wolkerstorfer, W. J. [1995] A linear maneuvering model for simulation of Slice hulls. Master's Thesis, Naval Postgraduate School, Monterey, California.

INITIAL DISTRIBUTION LIST

	No. Copies
1. Defense Technical Information Center 8725 John J. Kingman Rd., STE 0944 Ft. Belvoir, VA 22060–6218	2
2. Dubley Knox Library Naval Postgraduate School 411 Dyer Rd. Monterey, CA 93943–5101	2
3. Chairman, Code ME Department of Mechanical Engineering Naval Postgraduate School Monterey, California 93943	1
4. Professor Fotis A. Papoulias, Code ME/Pa Department of Mechanical Engineering Naval Postgraduate School Monterey, California 93943	3
5. Embassy of Greece Naval Attache 2228 Massachusetts Ave., N.W. Washington, D.C. 20008	2
6. Stavros I. Papanikolaou 13 Vomou St. Ano Kipseli, Athens 113-64 Greece	2
7. Naval Engineering Curricular Office, Code 34 Naval Postgraduate School Monterey, California 93943	1